



HAL
open science

The Absence of HIF-1 α Increases Susceptibility to Leishmania donovani Infection via Activation of BNIP3/mTOR/SREBP-1c Axis

Inês Mesquita, Carolina Ferreira, Diana Moreira, George Eduardo Gabriel Kluck, Ana Margarida Barbosa, Egídio Torrado, Ricardo Jorge Dinis-Oliveira, Luís Gafeira Gonçalves, Charles-Joly Beauparlant, Arnaud Droit, et al.

► To cite this version:

Inês Mesquita, Carolina Ferreira, Diana Moreira, George Eduardo Gabriel Kluck, Ana Margarida Barbosa, et al.. The Absence of HIF-1 α Increases Susceptibility to Leishmania donovani Infection via Activation of BNIP3/mTOR/SREBP-1c Axis. Cell Reports, 2020, 30, pp.4052 - 4064.e7. 10.1016/j.celrep.2020.02.098 . hal-03490073

HAL Id: hal-03490073

<https://hal.science/hal-03490073v1>

Submitted on 22 Aug 2022

HAL is a multi-disciplinary open access archive for the deposit and dissemination of scientific research documents, whether they are published or not. The documents may come from teaching and research institutions in France or abroad, or from public or private research centers.

L'archive ouverte pluridisciplinaire **HAL**, est destinée au dépôt et à la diffusion de documents scientifiques de niveau recherche, publiés ou non, émanant des établissements d'enseignement et de recherche français ou étrangers, des laboratoires publics ou privés.



Distributed under a Creative Commons Attribution - NonCommercial 4.0 International License

The absence of HIF-1 α increases susceptibility to *Leishmania donovani* infection via activation of BNIP3/mTOR/SREBP-1c axis

Inês Mesquita^{1,2}, Carolina Ferreira^{1,2}, Diana Moreira^{1,2,#}, George Eduardo Gabriel Kluck^{1,2,3,##}, Ana Margarida Barbosa^{1,2}, Egídio Torrado^{1,2}, Ricardo Jorge Dinis-Oliveira^{4,5,6}, Luís Gafeira Gonçalves⁷, Charles-Joly Beauparlant^{8,9}, Arnaud Droit^{8,9}, Luciana Berod¹⁰, Tim Sparwasser¹¹, Neelam Bodhale¹², Bhaskar Saha^{12,13,14}, Fernando Rodrigues^{1,2}, Cristina Cunha^{1,2}, Agostinho Carvalho^{1,2}, António Gil Castro^{1,2}, Jérôme Estaquier^{9,15,*}, Ricardo Silvestre^{1,2*,**}

¹ Microbiology and Infection Research Domain (MIRD), Life and Health Sciences Research Institute (ICVS), School of Medicine, University of Minho, 4710-057 Braga, Portugal;

² ICVS/3B's-PT Government Associate Laboratory, Braga/Guimarães, Portugal;

³ Laboratory of Lipid and Lipoprotein Biochemistry, Medical Biochemistry Institute, Federal University of Rio de Janeiro, 21941-901 Rio de Janeiro, Brazil;

⁴ Department of Public Health and Forensic Sciences, and Medical Education, Faculty of Medicine, University of Porto, 4200-319 Porto, Portugal;

⁵ Department of Sciences, IINFACTS - Institute of Research and Advanced Training in Health Sciences and Technologies, University Institute of Health Sciences (IUCS), CESPU, CRL, 4585-116 Gandra, Portugal;

⁶ UCIBIO-REQUIMTE, Laboratory of Toxicology, Department of Biological Sciences, Faculty of Pharmacy, University of Porto, 4050-313 Porto, Portugal;

⁷ Instituto de Tecnologia Química e Biológica António Xavier, Universidade Nova de Lisboa, 2780-157 Oeiras, Portugal.

⁸ Département de Médecine Moléculaire - Faculté de Médecine, Université Laval, Québec, QC G1V 0A6, Canada.

⁹ Centre de Recherche du CHU de Québec - Université Laval, Québec, QC G1V 4G2, Canada.

¹⁰ Institute of Infection Immunology, TWINCORE, Centre for Experimental and Clinical Infection Research, A Joint Venture between the Medical School Hannover (MHH) and the Helmholtz Centre for Infection Research (HZI), Hannover, Niedersachsen 30625, Germany.

¹¹ Department of Medical Microbiology and Hygiene, Medical Center of the Johannes Gutenberg-University of Mainz, Obere Zahlbacherstr, 6755131 Mainz, Germany

¹² National Centre for Cell Science, 411007 Pune, India;

¹³ Case Western Reserve University, 44106 Cleveland, Ohio, USA;

¹⁴ Trident Academy of Creative Technology, 751024 Bhubaneswar, Odisha, India;

¹⁵ INSERM U1124, Université de Paris, 75006 Paris, France.

Corresponding Authors *

Ricardo Silvestre

Life and Health Sciences Research Institute (ICVS), School of Medicine, University of Minho, Braga, Portugal; ICVS/3B's-PT Government Associate Laboratory, Braga/Guimarães, Portugal; e-mail: ricardosilvestre@med.uminho.pt

and

Jérôme Estaquier

Centre de Recherche du CHU de Québec, Université Laval, Québec, QC. INSERM U1124, Université de Paris, Paris, France; e-mail: estaquier@yahoo.fr

Current addresses

School of Biochemistry and Immunology, Trinity Biomedical Sciences Institute, Trinity College Dublin, 152-160 Pearse Street, Dublin 2, Ireland

McMaster University

Department of Biochemistry and Biomedical Sciences

Thrombosis and Atherosclerosis Research Institute (TaARI)

David Braley Cardiac, Vascular and Stroke Research Institute

Hamilton General Hospital Campus, Hamilton Health Sciences

237 Barton St E., Hamilton ON, Canada. L8L 2X2

**Lead contact: Ricardo Silvestre; ricardosilvestre@med.uminho.pt

Summary

Hypoxia-inducible factor-1 alpha (HIF-1 α) is considered a global regulator of cellular metabolism and innate immune cell functions. Intracellular pathogens as *Leishmania* have been reported to manipulate host cell metabolism. Herein, we demonstrate that myeloid cells from myeloid-restricted HIF-1 α deficient mice and individuals with loss-of-function *HIF1A* gene polymorphisms are more susceptible to *L. donovani* infection through increased lipogenesis. Absence of HIF-1 α leads to a defective of BNIP3 expression, resulting in the activation of mTOR and nuclear translocation of SREBP-1c. We observed the induction of lipogenic gene transcripts, as FASN, and lipid accumulation in infected HIF-1 α ^{-/-} macrophages. *L. donovani*-infected HIF-1 α -deficient mice develop hypertriglyceridemia and lipid accumulation in splenic and hepatic myeloid cells. Most importantly, our data demonstrate that manipulating FASN or SREBP-1c using pharmacological inhibitors significantly reduced parasite burden. As such, genetic deficiency of HIF-1 α is associated with increased lipid accumulation, which results in impaired host-protective anti-leishmanial functions of myeloid cells.

Introduction

Pathogen-induced hijacking of host cell metabolism results in the dampening of host defense mechanisms and is therefore considered an important host-pathogen interface (Naderer and McConville, 2008; McConville, 2016). Carbohydrate metabolism was initially proposed to play a central role in providing a nutrient-rich niche for pathogen multiplication and survival, as demonstrated in *Trypanosoma cruzi*, *T. brucei*, *Toxoplasma gondii* and *Leishmania donovani* infections (Caradonna *et al.*, 2013; Blume *et al.*, 2015; Ghosh *et al.*, 2015; Smith *et al.*, 2017). Other carbon sources, such as lipids, have also been proposed to contribute to the outcome of infection (Bozza *et al.*, 2009). Dysregulated lipid metabolism poses a social health problem worldwide due to the high prevalence of intertwined pathologies such as obesity, coronary heart disease, nonalcoholic fatty liver disease and diabetes. In the past few years, these pathologies have been gaining relevance in developing countries burdened by infectious diseases. These recently found nutritional alterations may favor pathogen dissemination, which poses a new challenge in the clinics.

Hypoxia-inducible factor 1 alpha (HIF-1 α) was initially identified as an oxygen-sensitive transcription factor involved in the regulation of the homeostatic response to hypoxia (Weidemann and Johnson, 2008; Thompson, 2016; Choudhry and Harris, 2017). In innate immune cells, HIF-1 α activation in response to pathogen-associated molecular patterns (PAMPs) (Peyssonnaud *et al.*, 2007; Spirig *et al.*, 2010; Cheng *et al.*, 2014) or pathogenic agents (Werth *et al.*, 2010) reprograms both carbohydrate and lipid metabolism and establishes an inflammatory phenotype (Palazon *et al.*, 2014). We and others previously reported that in *Leishmania*-infected macrophages, metabolism of carbohydrate and lipid is altered (Rabhi *et al.*, 2012; Moreira *et al.*, 2015) and HIF-1 α expression is upregulated (Degrossoli *et al.*, 2007; Singh *et al.*, 2012; Alonso *et al.*, 2019). Despite the implications for the metabolic networks in the immune functions of macrophages (Na *et al.*, 2016), the impact of HIF-1 α in the immune-metabolic regulation of macrophages, as modeled here with *Leishmania donovani* infection, remains elusive.

Herein, we demonstrate that HIF-1 α is a resistance factor against experimental visceral leishmaniasis (VL) caused by *Leishmania donovani*. The analysis of three distinct mouse strains with disparate susceptibility to the infection demonstrated that HIF-1 α expression is positively associated with the capacity to resist VL. To further dissect the role of this transcription factor, a murine model of myeloid HIF-1 α

deficiency (mHIF-1 α ^{-/-} mice) was used to explore the association between HIF-1 α expression and infection outcome. Among the few genes altered between infected HIF-1 α ^{-/-} and WT myeloid cells, the absence of HIF-1 α prevented BCL2-interacting protein 3 (BNIP3) upregulation, resulting in mammalian target of rapamycin (mTOR) activation. Consequently, sterol regulatory element-binding protein-1c (SREBP-1c) is activated leading to the up-regulation of key lipogenic enzymes, acetyl-CoA carboxylase (ACC) and fatty acid synthase (FASN), thus contributing to fatty acid synthesis. *L. donovani*-infected mHIF-1 α ^{-/-} mice developed a dysregulated lipid metabolism leading to lipid accumulation in both liver and spleen, thus favoring parasite multiplication. Pharmacological inhibition of FASN and SREBP-1c significantly reduced the susceptibility to infection and lipid dysregulation, demonstrating the causal relationship between HIF-1 α , lipid accumulation and *L. donovani* susceptibility. Furthermore, by associating the single nucleotide polymorphism (SNP) rs2057482 in human *HIF1A* gene with lower levels of HIF-1 α , we demonstrated the clinical relevance of this SNP during a protozoan infection.

Results

HIF-1 α expression is associated with increased resistance against *Leishmania donovani* infection.

As HIF-1 α ^{-/-} macrophages are more susceptible to *Leishmania major* infection (Schatz *et al.*, 2016), we first evaluated HIF-1 α transcription levels during *in vivo* *L. donovani* infection of three mouse strains with distinct outcomes to visceral leishmaniasis (VL); BALB/c as susceptible, 129/Sv as resistant and C57BL/6 as intermediate resistant hosts (Bodhale *et al.*, 2018). Splenic HIF-1 α transcription levels positively correlated with increased resistance to infection: the resistant 129/Sv mice had the highest levels of HIF-1 α transcription, whereas C57BL/6 mice had less HIF-1 α transcripts and BALB/c mice had the lowest HIF-1 α expression (figure 1A). To further dissect the role of this transcription factor during infection, we took advantage of myeloid-restricted HIF-1 α ^{-/-} mice (mHIF-1 α ^{-/-}), in which LysM Cre-specific deletion affects mostly monocytes, mature macrophages and neutrophils (Abram *et al.*, 2014). Although *L. donovani*-infected peritoneal macrophages from both WT and mHIF-1 α ^{-/-} mice displayed a similar level of phagocytosis (figure 1B), we observed at 5 days post-infection that parasite viability increases in HIF-1 α ^{-/-} macrophages when compared with WT counterparts (figure 1C). As expected, HIF-1 α activation with iron-chelating agent deferoxamine (DFX) resulted in lower parasite viability in WT macrophages and no alteration in mHIF-1 α ^{-/-} macrophages. We observed similar results with a distinct *L. donovani* strain or using a second visceral *Leishmania* species, *L. infantum* (figure S1A). To determine if *L. donovani* parasites display preferential tropism towards WT or HIF-1 α ^{-/-} macrophages, which could explain alterations in parasite viability, we co-cultured CD45.1 WT and CD45.2 HIF-1 α ^{-/-} macrophages and infected them with CFSE-labelled promastigotes. No differences were found in the percentage of phagocytosis between WT and HIF-1 α ^{-/-} macrophages (figure S1B) indicating that both macrophages comparably internalize the parasites. Yet, higher parasite viability was observed in HIF-1 α ^{-/-} macrophages (figure 1D) suggesting HIF-1 α as a host-protective factor against infection. The analysis of prototypical M1-like (*Cxcl9* and *Nos2*) and M2-like (*Arg1* and *Fizz1*) genes (Murray *et al.*, 2014) showed that the absence of HIF-1 α drives infected macrophages towards an anti-inflammatory phenotype, as shown by decreased *Cxcl9* and increased *Fizz1* transcriptional levels (figure 1E). Furthermore, infected HIF-1 α ^{-/-} macrophages display an imbalance in inflammation with lower levels

of IL-6 and TNF- α and higher levels of IL-10 (figure 1F). Altogether, our results indicate that HIF-1 α levels inversely associate with *Leishmania* infection.

***L. donovani* infected HIF-1 α ^{-/-} macrophages failed to upregulate BNIP3 leading to the activation of the mTOR signaling pathway**

To further dissect the role of HIF-1 α , we analyzed macrophage transcriptome through RNA sequencing at 6h post-infection. We only found 41 differentially regulated genes when comparing infected mHIF-1 α ^{-/-} and WT myeloid cells, with 27 downregulated and 14 upregulated in HIF-1 α ^{-/-} macrophages (figure 2A). No major changes were observed between uninfected macrophages, suggesting that HIF-1 α plays a minor role in macrophage basal phenotype (figure S2). Given that HIF-1 α is a transcription factor, we focused on the genes and pathways downregulated in *L. donovani*-infected mHIF-1 α ^{-/-} compared to WT. We found 7 downregulated pathways in the absence of HIF-1 α , mostly related to cell response to hypoxia as expected (figure 2B). Among the gene transcripts, we found that BCL2/adenovirus E1B 19-kDa-interacting protein 3 (BNIP3) was distinctively expressed in infected WT and HIF-1 α ^{-/-} macrophages (figure 2C). A quantitative PCR analysis confirmed that *Bnip3* transcriptional levels reach a maximum at 6 to 8 hours post-infection with viable *L. donovani* in WT macrophages, while *Bnip3* fails to be expressed in the absence of HIF-1 α (figure 2D). Furthermore, by western blot, lower BNIP3 levels were found in HIF-1 α ^{-/-} macrophages when compared to WT macrophages 10 hours post-infection (figure 2E).

As BNIP3 has been shown to contribute for the repression of mTOR via interaction with Ras-related GTPase Rheb (Li *et al.*, 2007), we investigated whether the absence of HIF-1 α was associated with the activation of p70 S6 kinase, a downstream target of mTOR. For that, we evaluated by western blot the phosphorylation status of p70 S6 kinase. We observed an increase in p70 S6K phosphorylation in HIF-1 α ^{-/-} macrophages, 10 hours post-infection (figure 2F), indicating that the mTOR pathway is activated in the absence of HIF-1 α . Further, a time dependency on mTOR activation was observed in *L. donovani* infected HIF-1 α ^{-/-} macrophages, as increased phosphorylation of p70 S6 kinase is not observed prior to 10 hours and is maintained until 24 hours post-infection (figure S3A). Next, we sought to understand if BNIP3 was responsible for controlling mTOR activation. siRNA

against BNIP3 (figure 2G) induce p70 S6K phosphorylation in WT macrophages infected with *L. donovani* (figure 2H), demonstrating that BNIP3 represses mTOR pathway in *L. donovani*-infected macrophages. Thus, our results support the idea that the absence of HIF-1 α by impairing BNIP3 expression induces the activation of mTOR during *L. donovani* infection.

SREBP1c activation in HIF-1 α ^{-/-} macrophages is responsible for *de novo* lipogenesis and increased *in vitro* susceptibility to *L. donovani* infection

Previous works have showed that activation of the mTOR pathway positively regulates the activity of the SREBP-1c transcription factor (Porstmann *et al.*, 2008; Düvel *et al.*, 2010). SREBP-1c is well known to bind to the promoter regions of lipogenic genes, thus inducing lipid synthesis (figure S3B). Although no differences were found in the transcriptional levels of the *Srebp1c* gene between infected WT and HIF-1 α ^{-/-} macrophages (figure S3C), we observed a significantly increased nuclear localization of this protein in infected HIF-1 α ^{-/-} macrophages compared to WT (figure 3A and S3D-E). As SREBP-1c activation is associated with increased lipid synthesis (Chang *et al.*, 2006; Sone *et al.*, 2015), we started by assessing any potential lipid accumulation during infection. A semi-quantitative analysis by high performance thin layer chromatography (HPTLC) showed a significant increase of distinct lipid families, such as free fatty acids and triacylglycerol, in infected HIF-1 α ^{-/-} macrophages (figure S4A-B), suggesting a *Leishmania*-driven lipid accumulation in the absence HIF-1 α . In opposition, activation of HIF-1 α in WT macrophages using deferoxamine (DXF) led to reduced lipid accumulation (figure S4C). Corroboratively, infected HIF-1 α ^{-/-} macrophages had increased intracellular neutral lipids, even in co-culture with WT macrophages (figure 3B-D). Overall, acetyl-CoA is a convergent metabolite from different carbon sources metabolism, namely glucose, glutamine, acetate and lactate, that can fuel lipid synthesis. Interestingly, we observed a significantly increased acetate concentration in *L. donovani*-infected HIF-1 α ^{-/-} macrophages, which is reduced in the presence of the SREBP-1c inhibitor fatostatin A (figure 3E-F). Nuclear magnetic resonance (NMR) analysis confirmed increased uptake of 2-¹³C-labelled acetate and its incorporation on the lipid fraction of infected HIF-1 α ^{-/-} macrophages (figure 3G and S5A-B), suggesting acetate uptake as a result of enhanced fatty acid synthesis in infected HIF-1 α ^{-/-} macrophages. Additionally, increased transcriptional levels of *Slc16a3* gene that codes for monocarboxylate transporter 4 (MCT4), were observed in

infected HIF-1 α ^{-/-} macrophages, which is in accordance with a higher acetate uptake in the absence of HIF-1 α (figure 3H). To further confirm that extracellular acetate is an additional source for lipid synthesis, macrophages were cultured in a medium supplemented with dialyzed fetal bovine serum (dFBS), which is deprived of acetate (figure 3I). A significant reduction of intracellular neutral lipids was observed in *L. donovani*-infected HIF-1 α ^{-/-} macrophages cultured in acetate deprivation (figure 3J). Medium supplementation with acetate (5 mM) led to a significant neutral lipid accumulation in both WT and HIF-1 α ^{-/-} macrophages (figure 3J), providing a causal link between acetate consumption and lipid accumulation in macrophages infected with *L. donovani*.

Following the hypothesis that lipogenesis is occurring in *L. donovani* infected HIF-1 α ^{-/-} macrophages, we analyzed the levels of fatty acid synthase (*Fasn*) and acetyl-CoA carboxylase (*Acaca*), which are two key enzymes from the *de novo* fatty acid synthesis (figure S4D). These two genes were found to be increased in infected HIF-1 α ^{-/-} macrophages (figure 4A). Inhibition of upstream players mTOR and SREBP-1c, with rapamycin and fatostatin A, respectively, abolished the induction of *Fasn* and *Acaca* transcription observed in infected HIF-1 α ^{-/-} macrophages (figure 4A). The protein levels of FASN were consistently increased in infected HIF-1 α ^{-/-} macrophages (figure 4B). Moreover, flow cytometric analyses of palmitate internalization revealed no difference between WT and HIF-1 α ^{-/-} macrophages, corroborating lipogenesis as the main source of lipid accumulation (figure S4E). To address the causal relationship between lipogenesis and increased parasite growth and survival, we inhibited FASN and ACC with C75 and Soraphen A (SorA), respectively. Both treatments led to a reduction in parasite viability observed in HIF-1 α ^{-/-} cells (figure 4C), along with a decrease of approximately 25% of total intracellular lipids (figure S4F). Moreover, fatostatin A significantly reduced the parasite viability in HIF-1 α ^{-/-} macrophages (figure 4D), indicating that lipid biogenesis is likely associated to an upstream activation of FASN by SREBP-1c and leading to the establishment of a permissive niche for parasite proliferation and survival. Of note, although lipid storage and metabolism have been associated with HIF-2 activation (Rankin *et al.*, 2009; Liu *et al.*, 2014), we observed a negligible role for HIF-2 in lipid metabolism in infected macrophages (data not shown). These data demonstrate that *Leishmania* infection of HIF-1 α ^{-/-} macrophages *in vitro* is associated with lipogenesis that contributes to parasite growth.

HIF-1 α deficiency in the myeloid compartment correlates with *in vivo* lipid accumulation and higher *L. donovani* burdens

To determine the *in vivo* impact of HIF-1 α on parasite growth and lipid metabolism, we infected mHIF-1 $\alpha^{-/-}$ mice with *L. donovani*. Assessment of parasite load at the indicated time-points revealed that mHIF-1 $\alpha^{-/-}$ mice exhibited higher parasite burdens in the spleen and in the liver, compared to WT mice (figure 5A). Splenic and hepatic myeloid cells (gated on CD11b⁺Ly6C⁺) of infected mHIF-1 $\alpha^{-/-}$ mice displayed higher intracellular neutral lipids (figure 5B). A similar phenotype regarding parasite burden and lipid accumulation in parasitized organs was observed using a ten-fold lower *L. donovani* inoculum (figure S6A-B), demonstrating that the observed phenotype is independent of the initial inoculum. We also observed a positive correlation between splenic intracellular lipid content and parasite burden in two week-infected mHIF-1 $\alpha^{-/-}$ mice (figure 5C). Corroborating our *in vitro* observations, spleen homogenates from infected mHIF-1 $\alpha^{-/-}$ mice showed significant higher transcriptional levels of *Fasn* and *Acaca* (figure 5D). We observed a pronounced Oil Red O staining in frozen liver sections from infected mHIF-1 $\alpha^{-/-}$ mice, indicating generalized lipid accumulation (figure 5E). Two weeks post-infection, higher levels of cholesterol and triglycerides were detected in the serum of mHIF-1 $\alpha^{-/-}$ mice (figure 5F). The levels of HDL were decreased in infected mHIF-1 $\alpha^{-/-}$ mice while LDL levels remained unaltered (figure S6C). Similar observations regarding lipid accumulation in the serum were made at eight weeks post-infection (data not shown). As lipid dysregulation may be a consequence of liver damage, we analyzed the levels of aspartate and alanine transaminase (AST and ALT, respectively) as biomarkers for hepatic injury. Both were significantly elevated in infected mHIF-1 $\alpha^{-/-}$ mice at two weeks post-infection (figure 5G). Altogether, these results suggest that the absence of HIF-1 α facilitates parasite growth through lipid accumulation and dysregulation of its metabolism.

Targeting lipid biosynthesis *in vivo* reverts mHIF-1 $\alpha^{-/-}$ -associated susceptibility

As lipids accumulated during experimental infection of mHIF-1 $\alpha^{-/-}$ mice, we then hypothesized that the blockade of lipid synthesis would modulate the susceptibility phenotype and improve the outcome of the infection. We infected both WT and mHIF-1 $\alpha^{-/-}$ mice and treated the animals with FASN or SREBP-1c inhibitors C75 and fatostatin A, respectively (figure 6A). We observed that the FASN or SREBP-1c blockade reverted the observed susceptibility in mHIF-1 $\alpha^{-/-}$ mice, as parasite burden

was significantly reduced in both spleen and liver (figure 6B). *L. donovani*-infected and treated mHIF-1 α ^{-/-} mice displayed lower levels of cholesterol and triglycerides in the serum, as compared to the infected mice on placebo (figure 6C). The levels of ALT, AST, creatine and urea in the serum remained unchanged upon drug treatment, suggesting that acute treatment with C75 and fatostatin A is not associated with liver or kidney toxicity (figure S6D-E). Our data suggest that lipid biosynthesis occurring in infected mHIF-1 α ^{-/-} mice contributes for the increased susceptibility towards *L. donovani* infection.

Genetic variation in human *HIF1A* promotes increased parasite viability and lipid accumulation

Genetic variations in human *HIF1A* have been reported to influence several diseases (Hlatky *et al.*, 2007; Kim *et al.*, 2008; Guo *et al.*, 2015; Wang *et al.*, 2016). It has been described that mRNA expression level of *HIF1A* is lower in individuals carrying CT/TT genotypes at rs2057482 compared to CC carriers. This SNP is localized in the 3'-UTR region of *HIF1A* and close to two predicted microRNA binding sites (hsa-miR-199a/b-5p and hsa-miR-340) (Guo *et al.*, 2015; Wang *et al.*, 2016). Therefore, we decided to assess if human monocyte-derived macrophages from healthy donors carrying different genotypes displayed distinct *L. donovani* infection outcomes. First and consistent with a previous report (Wang *et al.*, 2016), we observed that the transcription levels of *HIF1A* gene were decreased in macrophages with the CT/TT genotype, when compared to cells from CC carriers (figure 7A). Furthermore, our results showed an increase in parasite viability in CT/TT macrophages, associated with lower levels of *HIF1A* (figure 7B). We also demonstrated that *HIF1A* levels were inversely correlated with parasite viability (figure 7C; p=0.0362; r=-0.3777) and intracellular neutral lipids (figure 7D; p=0.0057; r=-0.4777), while parasite viability correlated positively with intracellular neutral lipids (figure 6E; p=0.0150; r=0.3929). Treatment of infected macrophages from CT/TT donors with C75 led to a significant decrease in parasite viability, in contrast to what occurs with CC macrophages (figure 7F-G). These results unveil a major breakthrough in our understanding of human susceptibility to parasite infection associated with a genetic variation in human *HIF1A* expression that can be reverted by inhibiting lipid accumulation through FASN blockage.

Discussion

A growing body of evidence suggests that the metabolic status of a host cell has pivotal importance for building up an adequate immune response. However, successful pathogens have in turn evolved and acquire complex and efficient methods to subvert and evade immune responses by manipulating host cell metabolism. Whereas several groups have proposed a role for HIF-1 α in regulating protozoan infections (Degrossoli *et al.*, 2007; Singh *et al.*, 2012; McGettrick *et al.*, 2016; Schatz *et al.*, 2016; Alonso *et al.*, 2019), the mechanisms behind it remain elusive. In this study, we demonstrate the contributing role of myeloid HIF-1 α in the modulation of lipid metabolism during *L. donovani* infection. We show that the absence of myeloid HIF-1 α dysregulates lipid metabolism via BNIP3/mTOR/SREBP-1c axis upon *L. donovani* infection. This survival advantage to the parasite is reverted by the blockade of lipid synthesis. Finally, we demonstrate that individuals carrying an *HIF1A* SNP (rs2057482) display lower transcript levels of *HIF1A* in macrophages and are more susceptible to *L. donovani* infection, which positively correlates with increased lipogenesis.

HIF-1 α was initially described as a master transcriptional factor in response to hypoxia and a key mediator of glycolysis (Lu, Forbes and Verma, 2002; Lee *et al.*, 2004; Marin-Hernandez *et al.*, 2009). Recent evidences suggest that this factor is also essential in regulating the production of inflammatory cytokines and chemoattractive factors by macrophages and endothelial cells (Imtiyaz and Simon, 2010; Palazon *et al.*, 2014). PAMPs, including Toll-like receptor (TLR) agonists, induce an HIF-1 α -dependent production of inflammatory cytokines in pro-inflammatory macrophages (Cramer *et al.*, 2003; Rius *et al.*, 2008; Nicholas and Sumbayev, 2009; Palsson-Mcdermott *et al.*, 2015). By contrast, anti-inflammatory macrophages display a more oxidative metabolic profile, characterized by the utilization of oxidative phosphorylation and fatty acid oxidation (FAO), for which HIF-1 α has a minor role (Vats *et al.*, 2006; Nomura *et al.*, 2016). The absence of HIF-1 α could hypothetically drive macrophage polarization towards an anti-inflammatory and permissive profile, characterized by lower levels of nitric oxide (NO) and reactive oxygen species (ROS), which weakens anti-*Leishmania* response (Rodrigues *et al.*, 2016; Schatz *et al.*, 2016). In accordance with this, we observed that infected, susceptible BALB/c mice display constant levels of HIF-1 α through the course of infection. In opposition, resistant mouse strains, as 129/SV and C57BL/6, exhibit an induction of HIF-1 α transcription,

suggesting that HIF-1 α expression and activation is relevant for the establishment of an effective anti-*Leishmania* responses (figure 1A). Therefore, the levels of HIF-1 α may dictate host susceptibility or resistance, as the absence of this factor in CD11b⁺ population during *L. donovani* infection results in a higher number of intracellular parasites (figure 1C). Accordingly, we observed a decreased NO production on infected HIF-1 α ^{-/-} macrophages when compared to WT counterpart (figure S7A), demonstrating that the absence of this factor leads to reduced host microbicidal mechanisms, as previously reported (Schatz *et al.*, 2016). The observed susceptibility phenotype contrasts with a previous work in which the absence of HIF1 α in CD11c⁺ cells (C57BL/6 Cd11c-Cre^{+/-}) rendered a protective phenotype (Hammami *et al.*, 2017). We assume that the differences observed are mainly related with the type of cells deficient for HIF1 α .

In addition to this, a shift in the literature-based prototype transcript markers towards an anti-inflammatory phenotype, as well as a dysregulated balance between pro- and anti-inflammatory cytokines was observed in the absence of HIF-1 α (figure 1E-F). However, additional host-driven mechanisms are thought to be implied in the observed susceptibility in the absence of HIF-1 α . Considering the importance of an adequate metabolic environment for the correct development of immune responses, we hypothesized that HIF-1 α deficiency in the CD11b compartment could severely influence host metabolism with a consequent impact on infection outcome. Although seminal works in cancer metabolism have elucidated the role of HIF-1 α in glycolysis, a quite controversial role for this factor in lipid metabolism has been established for distinct models of pathogenesis. While a positive association between lipid accumulation and HIF-1 α activation has been explored (Nath *et al.*, 2011; Bensaad *et al.*, 2014; Du *et al.*, 2017), this process appears to be cell- and context-specific, as other studies have demonstrated the opposite (Zhang *et al.*, 2010; Nishiyama *et al.*, 2012; Rahtu-Korpela *et al.*, 2014, 2016). In our work, we found that the absence of HIF-1 α during *L. donovani* infection is associated with an increased lipogenesis driven by an up-regulation of ACC and FASN (figure 3 and 4). We ascribed the increased growth of *L. donovani* to a higher lipogenesis, as pharmacological inhibition of this pathway reverted the observed phenotype and reduced parasite growth (figure 4C and 6B). The blockage of fatty acid synthesis has already been explored as a therapeutic approach in several diseases. Indeed, blockade of FASN with C75 has been explored in the context of sepsis (Idrovo *et al.*, 2015), hemorrhagic shock (Kuncewitch *et al.*, 2016), colitis

(Matsuo *et al.*, 2014) and cancer (Kuhajda *et al.*, 2000; Flavin *et al.*, 2010), while the ACC inhibitor sorafenib was shown to have an impact in experimental autoimmune encephalomyelitis (Berod *et al.*, 2014) and graft-versus-host disease (Raha *et al.*, 2016). Therefore, these molecules could be included in the therapeutics arsenal against VL.

Given that HIF-1 α is a transcriptional factor, we performed a RNA-sequencing approach of infected WT and HIF-1 α ^{-/-} gene expression profile to ascertain the mechanism behind the observed phenotype. Our results show that, in the absence of HIF-1 α , infected macrophages down-regulate several pathways associated with hypoxia (figure 2B). Interestingly, we observed that *Bnip3* was the most significantly altered gene, which was up-regulated in infected WT macrophages, whilst no transcriptional changes were observed in HIF-1 α ^{-/-} macrophages (figure 2C). This gene has a promoter region that is a direct target of transcriptional activation via HIF-1 α , which is steadily induced in hypoxia (Chinnadurai, Vijayalingam and Gibson, 2008). Alongside with this, BNIP3 has been shown to repress mTORC1 activation via interaction with Rheb GTPase (Li *et al.*, 2007), which suggests that BNIP3 directly interferes with cellular metabolism through the modulation of mTOR function. Accordingly, our results show that in the absence of HIF-1 α , BNIP3 expression is maintained at basal levels and, consequently, mTOR is activated, as observed by the increased phosphorylation status of mTOR direct target S6 kinase (figure 2F). Of note, even though BNIP3 is a pro-apoptotic protein, we found no differences on the levels of autophagy or cell death between *L. donovani* infected WT and HIF-1 α ^{-/-} macrophages (data not shown). One of the most important functions regulated by mTOR is the activation of SREBP-driven lipid synthesis, which is crucial for the maintenance and establishment of cell growth programs (Laplante and Sabatini, 2009; Caron, Richard and Laplante, 2015; Mao and Zhang, 2018). SREBP-1c is a master promotor of lipogenesis via activation of a specific transcriptional program (Horton, Goldstein and Brown, 2002; Joseph *et al.*, 2002; Eberlé *et al.*, 2004; Xiao and Song, 2013). Consistently, we demonstrated that the activation of fatty acid synthesis is driven by mTOR/SREBP-1c activation as blockage of these factors with rapamycin or fatostatin A reverts lipid accumulation and, consequently, the increased susceptibility of mHIF-1 α ^{-/-} mice (figure 4A and 6B). Therefore, this represents a different avenue in our understanding of host-pathogen interaction in which BNIP3 may play a major role in the susceptibility of parasite infection.

We observed that acetate was used as an additional carbon source for the lipid synthesis and accumulation in HIF-1 α ^{-/-} macrophages, which is consistent with an increased acetate uptake in infected HIF-1 α ^{-/-} macrophages. The role of acetate in promoting lipid biogenesis as well as its incorporation in lipid droplets in both mammalian cells and pathogenic agents has already been described in certain experimental conditions (Howard, 1977; Riviere *et al.*, 2009; Liu, Qiao and Stephanopoulos, 2016). The synthesis of acetyl-CoA from acetate is known to be induced via SREBP-1c activation, which indicates a role for acetate in lipogenesis. Consistently, isotope-labelling experiments using sodium acetate-2-¹³C showed that infected mHIF-1 α ^{-/-} macrophages have an increased uptake of acetate and incorporation in the lipid fraction (figure 3G and S5A-B), explaining the increased lipogenic flux in these cells. We also observed an increased expression of MCT4 that has been shown to uptake lactate, pyruvate or acetate. Conversely to acetate, pyruvate and lactate supplementation did not lead to increased lipid accumulation in HIF-1 α ^{-/-} infected macrophages (fig 3J and data not shown). Furthermore, although we observed a decrease in lipid accumulation in infected HIF-1 α ^{-/-} macrophages cultured in the absence of acetate (fig 3J), we cannot exclude the contribution of other sources for the observed phenotype.

Rabhi and colleagues demonstrated that *Leishmania* parasites co-localize with intracellular lipid droplets (Rabhi *et al.*, 2012, 2016). However, whether lipids are used as a high energy source to feed amastigotes (De Cicco *et al.*, 2012) or as a shield to protect them from host microbicidal mechanisms (Bailey *et al.*, 2015) remains to be addressed. Our preliminary data show that infected HIF-1 α ^{-/-} macrophages display higher levels of lipid peroxidation (data not shown) suggesting a role for lipids in protecting *L. donovani* parasites from killing by host cells. The mechanistic events that explain how the absence of HIF-1 α results in the increased activation of these lipogenic factors remain to be deciphered. One hypothesis could be that an initial peak of ROS production by infected HIF-1 α ^{-/-} macrophages could trigger SREBP-1c activation and consequent lipid production (Liu *et al.*, 2015). No major alterations were observed in peroxynitrite and superoxide anion accumulation in infected macrophages early after infection (data not shown), although other sources, as mitochondrial ROS production, remain to be addressed. Alternatively, HIF-1 α may induce lipogenesis due to activation of upstream TLR2 and TLR4, which are triggered upon *Leishmania* infection (Becker *et al.*, 2003; Kropf *et al.*, 2004; Tuon *et al.*, 2008; Silvestre *et al.*, 2009) and have been

associated to macrophage lipid accumulation (Feingold *et al.*, 2012). Indeed, TLR2 and TLR4 activation with Pam3CSK4 and LPS, respectively, increases intracellular neutral lipids in the absence of HIF-1 α (figure S7B). Thus, HIF-1 α may restrict lipid accumulation through alterations of TLR signaling, although this hypothesis requires further studies.

Genetic variations in human *HIF1A* have been reported to influence the developing risk and prognosis of many types of human malignancies, such as cancer and coronary artery disease (Hlatky *et al.*, 2007; Kim *et al.*, 2008; Guo *et al.*, 2015; Wang *et al.*, 2016). Among *HIF1A* polymorphisms, rs2057482 has been associated with a lower expression of HIF-1 α . This SNP is localized in the 3'UTR region of the *HIF1A* gene, a site which has been demonstrated to be under the control of miR-199a, capable of repressing HIF-1 α transcription (Wang *et al.*, 2016). Our results demonstrated that genetic variation in *HIF1A* may contribute to regulate parasite growth in macrophages. Thus, in macrophages from individuals with the CT/TT genotype at rs2057482, in which HIF-1 α expression is lower, parasite growth is higher than the observed in macrophages from CC carriers. Moreover, we observed that lower levels of HIF-1 α are positively correlated with higher levels of lipids (figure 7). High frequencies of the rs2057482 SNP in regions with a high number of VL cases (Asia~34.88% and Sub-Saharan Africa~46.02%; available on <https://www.ncbi.nlm.nih.gov/snp>) may identify HIF-1 α as a major host factor that regulates resistance and susceptibility to VL. Therefore, it would be of interest to perform clinical studies assessing the impact of such polymorphism in patients.

In conclusion, our data identified HIF-1 α as a host-protective factor against *L. donovani* infection. Absence of HIF-1 α results in elevated lipogenesis, creating an intracellular milieu conducive for parasite growth and survival, thus supporting the hypothesis that lipid accumulation is important for *Leishmania* survival within host cells (Rabhi *et al.*, 2016; Rodríguez *et al.*, 2017; Semini *et al.*, 2017). Our demonstration that pharmacological compounds targeting lipid synthesis modulate susceptibility to parasite infection that may aid the development of therapies for VL cure.

Acknowledgments

This work was supported by the Northern Portugal Regional Operational Programme (NORTE 2020), under the Portugal 2020 Partnership Agreement, through the European Regional Development Fund (FEDER) (NORTE-01-0145-FEDER-000013), Project LISBOA-01-0145-FEDER-007660 (Microbiologia Molecular, Estrutural e Celular) funded by FEDER funds through COMPETE2020 - Programa Operacional Competitividade e Internacionalização (POCI) and the Fundação para a Ciência e Tecnologia (FCT) (contracts SFRH/BD/120127/2016 to IM, PD/BDE/127830/2016 to CF, SFRH/BD/120371/2016 to AMB, IF/01147/2013 to RJDO, SFRH/BPD/111100/2015 to LGG, IF/01390/2014 to ET, IF/00735/2014 to AC, SFRH/BPD/96176/2013 to CC and IF/00021/2014 to RS), and Infect-Era (project INLEISH). JE also thank the Canada Research Chair program for financial assistance. BS thanks CWRU/UH Centre for AIDS Research (NIH Grant Number P30 AI036219) and DBT (BT/In/Infect-eRA/33/BS/2016-2017). The NMR data was acquired at CERMAX, ITQB-NOVA, Oeiras, Portugal with equipment funded by FCT, project AAC 01/SAICT/2016. We thank Dr. Cláudia Nobrega and Dr. Margarida Correia Neves for providing the Ly5.1 mice and Dr. Nuno Alves for the cell sorting.

Author Contributions

Conceptualization and methodology: IM, DM, BS, FR, CC, AC, AGC, JE and RS; Investigation: IM, CF, DM, GEGK, AMB, RJDO, LGG, NB, CC, and RS; Formal analysis: IM, CF, DM, GEGK, ET, RJDO, LGG, NB, AD, CJB, JE and RS; Visualization: IM, BS, JE, and RS; Writing – original draft: IM, BS, JE, and RS; Supervision: JE and RS; Resources: TS, LB, BS, JE and RS; Funding acquisition: BS, JE and RS.

Declaration of Interests

The authors declare no competing interests.

Figure Legends

Figure 1. HIF-1 α expression is associated with increased resistance against *Leishmania donovani* infection

(A) The *Hif1a* transcription levels were quantified on splenic extracts of uninfected and 14- and 28-days *L. donovani*-infected Balb/c, C57BL/6 and 129/SV mice; (B) Peritoneal macrophages from WT and mHIF-1 $\alpha^{-/-}$ mice were infected with CFSE-labelled promastigotes. Phagocytosis was assessed 4 hours post-infection by flow cytometry; (C) Peritoneal macrophages from WT and mHIF-1 $\alpha^{-/-}$ were infected and parasite burden was evaluated by quantifying *L. donovani* viability at 5 days post-infection. Deferoxamine (DFX) treatment was performed 24 hours post-infection; (D) An equal amount of WT CD45.1 and HIF-1 $\alpha^{-/-}$ CD45.2 macrophages were co-culture and infected with *L. donovani*. Parasite viability was determined. Lines represent the cells cultured in the same well; (E) qPCR analysis of the transcriptional levels of *Cxcl9*, *Nos2*, *Arg1* and *Fizz1* 24 hours post-infection; (F) Cytokines (TNF- α , IL-6 and IL-10) were quantified on the supernatant of both WT and HIF-1 $\alpha^{-/-}$ by ELISA. Data is shown as mean \pm SD; n=5-7 mice/group. *p<0.05; **p<0.01; ***p<0.001; NS – not significant.

Figure 2. *L. donovani* infected HIF-1 $\alpha^{-/-}$ macrophages failed to upregulate BNIP3 leading to the activation of the mTOR signaling pathway

(A) Genome-wide transcriptome analysis of murine WT and HIF-1 $\alpha^{-/-}$ macrophages infected with *L. donovani* for 6 hours. Expression values (log₂ fold) were plotted against the adjusted P value (-log₁₀) for the difference in expression. Annotated numbers indicate genes with significant differential expression: upregulated (red=14) or downregulated (blue=27), 1.5 fold or more in infected HIF-1 $\alpha^{-/-}$ macrophages relative to infected WT cells; (B) Pathway analysis of significantly downregulated genes. The genes were divided into the top 8 most represented pathways. The number of differentially expressed genes in each pathway is annotated in each bar. (C) Genome-wide transcriptional profiles of murine WT and HIF-1 $\alpha^{-/-}$ macrophages infected with *L. donovani* (n=4-5). Expression of genes (right margins) is presented as centered and “scaled” log₂ fluorescence intensity. (D) qPCR analysis of the transcriptional levels of *Bnip3* 2, 6, 8 and 14 hours post-infection; (E) Western blot analysis and densitometry of BNIP3 and beta-actin; (F) Western blot analysis and densitometry of phospho-p70

S6K, total p70 S6K and beta-actin; (G) Western blot analysis and densitometry of BNIP3 and beta-actin, after siBNIP3 transfection; (H) Western blot analysis and densitometry phospho-p70 S6K, total p70 S6K and beta-actin, after siBNIP3 transfection.

Figure 3. SREBP1c activation in mHIF-1 α ^{-/-} is responsible for acetate-driven *de novo* lipid accumulation and susceptibility to infection

(A) Immunofluorescence confocal microscopy of *Leishmania*-infected WT or HIF-1 α ^{-/-} macrophages. At 24 hours post-infection, macrophages were fixed and probed with an anti-SREBP1c antibody; green, SREBP1c; blue, DNA (DAPI). White arrows point to *L. donovani* nucleus (B) Representative histogram of Bodipy 493/503 staining by flow cytometry at 5 days post-infection; (C) Intracellular neutral lipids in infected and uninfected WT and HIF-1 α ^{-/-} macrophages; (D) Intracellular neutral lipids in infected co-cultured WT CD45.1 and HIF-1 α ^{-/-} CD45.2 macrophages ; (E) Acetate quantification in intracellular extracts from infected WT and HIF-1 α ^{-/-} macrophages, 5 days post-infection. (F) Acetate quantification in intracellular extracts from infected HIF-1 α ^{-/-} macrophages in the absence or presence of fatostatin A; (G) Intracellular accumulation of the ¹³C label that was incorporated in 2-¹³C labeled acetate was determined in lysates from uninfected and *L. donovani*-infected WT or HIF1 α ^{-/-} peritoneal macrophages upon 24 hours by NMR; (H) qPCR analysis of the transcriptional levels of *Slc16a3* 24 hours post-infection; (I) Acetate concentration in RPMI media, supplemented with regular fetal bovine serum (FBS) or dialyzed FBS (dFBS); (J) WT or HIF-1 α ^{-/-} macrophages cultured in standard conditions (-), with dialyzed FBS (+ Dial. FBS) or in the presence of 5mM of acetate (+5mM acetate) were infected with *L. donovani*. Intracellular neutral lipids were quantified as abovementioned. Data is shown as mean \pm SD; n=4-11 mice/group. *p<0.05; **p<0.01; ***p<0.001.

Figure 4. Increased susceptibility to *Leishmania donovani* infection in the absence of HIF-1 α is associated with *de novo* lipid accumulation.

(A) qPCR analysis of the transcriptional levels of *Acaca* and *Fasn* 24 hours post-infection; (B) Western blot analysis and densitometry of FASN and beta-actin 24 hours post-infection; (C) *L. donovani* viability was assessed 5 days post-infection, upon C75 and sorafen A (SorA) treatment. (D) *L. donovani* viability was assessed 5 days post-

infection, after Fatostatin A treatment. Data is shown as mean \pm SD; n=4-15 mice/group. *p<0.05; **p<0.01; ***p<0.001.

Figure 5. HIF-1 α deficiency in the myeloid compartment correlates with higher *L. donovani* burdens and systemic lipid dysregulation. (A) Parasite burden in the spleen and liver of WT and mHIF-1 α ^{-/-} 2 and 8 weeks post-infection; (B) Quantification of intracellular neutral lipids by flow cytometry using Bodipy 493/503, on gated splenic and hepatic CD11b⁺ cells ; (C) Correlation between intracellular neutral lipids on CD11b⁺ cells and parasite burden in the spleen of mHIF-1 α ^{-/-} mice; (D) qPCR analysis of the transcriptional levels of *Acaca* and *Fasn* in spleen homogenates; (E) Liver sections with Oil Red O staining and H&E counterstaining; (F) Cholesterol and triglycerides and (G) ALT and AST levels on the spleen and liver extracts. All data from (B) to (G) were obtained with samples from WT and/or mHIF-1 α ^{-/-} 2 weeks post-infection. Data is shown as mean \pm SD; n=3-10 mice/group. *p<0.05; **p<0.01; ***p<0.001.

Figure 6. Targeting lipid anabolism reverts mHIF-1 α ^{-/-}-associated susceptibility. (A) Treatment scheme with C75 and fatostatin A (further detailed on M&M section). Mice were euthanized ten days post-infection; (B) Parasite burden in the spleen and liver of C75 and fatostatin A-treated and untreated WT and mHIF-1 α ^{-/-}; (C) Cholesterol and triglycerides levels on the serum of C75 and fatostatin A-treated and untreated WT and mHIF-1 α ^{-/-}. Data is shown as mean \pm SD; n=4-12 mice/group. *p<0.05; **p<0.01; ***p<0.001.

Figure 7. Genetic variation in human *HIF1A* promotes increased parasite viability and lipid accumulation. (A) qPCR analysis of the transcriptional levels of *HIF1A* in human macrophages from donors with the CC and CT/TT genotype at rs2057482; (B) *L. donovani* viability 5 days post-infection; (C) Correlation between parasite viability and *HIF1A* transcriptional levels, (D) *HIF1A* transcriptional levels and intracellular neutral lipids and (E) parasite viability and intracellular neutral lipids; (F, G) *L. donovani* viability after C75 treatment. Data is shown as mean \pm SD; **p<0.01.

KEY RESOURCES TABLE

REAGENT or RESOURCE	SOURCE	IDENTIFIER
Antibodies		
Brilliant Violet 785 anti-mouse NK-1.1 (clone PK136)	Biologend	Cat#: 108749
APC anti-mouse I-A/I-E (clone M5/114.15.2)	Biologend	Cat#: 107614
Brilliant Violet 605 anti-mouse CD11c (clone N418)	Biologend	Cat#: 117334
PE/Cy7 anti-mouse CD11b (clone M1/70)	Biologend	Cat#: 101216
Brilliant Violet 711 anti-mouse Ly-6G (clone 1A8)	Biologend	Cat#: 127643
PerCP/Cy5.5 anti-mouse Ly-6C (clone HK14)	Biologend	Cat#: 128012
APC anti-mouse CD45.2 (clone 104)	Biologend	Cat#: 109814
PE anti-mouse CD45.1 (clone A20)	Biologend	Cat#: 110708
Mouse monoclonal anti-fatty acid synthase (G-11)	Santa Cruz Biotechnology	Cat#: Sc-48357
Rabbit monoclonal anti-beta-actin (N-21)	Santa Cruz Biotechnology	Cat#: Sc-130656
Peroxidase AffiniPure Goat Anti-Rabbit IgG (H+L)	Jackson ImmunoResearch	Cat#: 111-035-144
Peroxidase AffiniPure Goat Anti-Mouse IgG (H+L)	Jackson ImmunoResearch	Cat#: 115-035-003
SREBP1 antibody	Novus Biologicals	Cat#: NB100-2215SS
Alexa Fluor 488 goat anti-rabbit IgG (H+L)	ThermoFisher Technologies	Cat#: A11008
BNIP3 Antibody (BH3 Domain Specific)	Antibodies Online	Cat#: ABIN388117
P70 S6 Kinase Antibody	Cell Signaling Technologies	Cat#: 9202S
Phospho-p70 S6 Kinase (Thr389) Antibody	Cell Signaling Technologies	Cat#: 9205S
HIF-1 α Antibody	Cell Signaling Technologies	Cat#: 14179S
Chemicals, Peptides, and Recombinant Proteins		
Dulbecco's Modified Eagle Medium (DMEM)	ThermoFisher Technologies	Cat#: 10938025
RPMI medium 1640	ThermoFisher Technologies	Cat#: 31870025
L-glutamine (200 mM)	ThermoFisher Technologies	Cat#: 25030081
HEPES buffer solution (1M)	ThermoFisher Technologies	Cat#: 15630056
Penicillin-Streptomycin (10 000U/ml)	ThermoFisher Technologies	Cat#: 15140122
Phosphate Buffered Saline (PBS) pH 7.4 (10x)	ThermoFisher Technologies	Cat#: 70011044
UltraPure Distilled Water Dnase/Rnase free	ThermoFisher Technologies	Cat#: 10977035
Oil Red O	Sigma-Aldrich	Cat#: O0625
Recombinant human M-CSF	Peptotech	Cat#: 300-25
Recombinant murine M-CSF	Peptotech	Cat#: 315-02
C 75	Tocris	Cat#: 2489
Fatostatin A	Tocris	Cat#: 4444
Deferoxamine Mesylate Salt	Sigma-Aldrich	Cat#: D9533
Soraphen A	Dr. Tim Sparwasser and Dr. Luciana Berod (TWINCORE)	N/A

Lipopolysaccharide from <i>Escherichia coli</i> O26:B6	Sigma-Aldrich	Cat#: L-8274
Pam3CSK4	Invivogen	Cat#: 112208-00-1
TRI reagent	Sigma-Aldrich	Cat#: T9424
Tissue-Tek O.C.T. compound	Sakura Finetek, VWR	Cat#: 4583
Complete EDTA-free Protease Inhibitor Cocktail Tablets	Roche	Cat#: 11873580001
Halt Protease and Phosphatase Inhibitor Cocktail (100x)	ThermoFisher Scientific	Cat#:78440
SuperSignal West Femto Maximum Sensitivity Substrate	ThermoFisher Scientific	Cat#: 34094
HiMark Pre-stained Protein Standard	ThermoFisher Scientific	Cat#: LC5699
PageRuler™ Prestained Protein Ladder, 10 to 180 kDa	ThermoFisher Scientific	Cat#: 26616
Phenol:Chloroform:Isoamyl Alcohol 25:24:1, Saturated with 10mM Tris, pH 8.0, 1mM	Sigma-Aldrich	Cat#: P3803
Formalin solution, neutral buffered, 10%	Sigma-Aldrich	Cat#: HT501128
Percoll	GE HealthCare	Cat#: 17-0891-01
Histopaque-1077	Sigma-Aldrich	Cat#: 10771
Chloroform	Carlo Erba Reagents	Cat#: 438603
Methanol	Sigma-Aldrich	Cat#: 34885-M
Hexane	Sigma-Aldrich	Cat#: 296090
Acetic acid glacial	Carlo Erba Reagents	Cat#: 401424
Diethyl ether	Sigma-Aldrich	Cat#: 676845
Paraformaldehyde	Sigma-Aldrich	Cat#: P6148
Sulfuric acid 96%	PanReac AppliChem	Cat#: 131058.1212
Copper (II) sulfate pentahydrate	Sigma-Aldrich	Cat#: C7631
Sodium phosphate dibasic dihydrate	Carlo Erba Reagents	Cat#: 480227
Corn Oil, delivery for fat-soluble compounds	Sigma-Aldrich	Cat#: C8267
Dimethyl sulfoxide	Sigma-Aldrich	Cat#: 276855
Albumin from bovine serum	Sigma-Aldrich	Cat#: A7906
Fetal Bovine Serum	ThermoFisher Scientific	Cat#: 10270106
Fetal Bovine Serum, dialyzed, US origin	ThermoFisher Scientific	Cat#: 26400044
Sodium acetate-2- ¹³ C	Cortecnet	Cat#: CC3395P
Sodium pyruvate (100 mM)	ThermoFisher Scientific	Cat#: 11360070
Sodium acetate	Sigma-Aldrich	Cat#: S-2889
Sodium DL-lactate	Sigma-Aldrich	Cat#: 71720-25G
Opti-MEM Reduced Serum Media	ThermoFisher Scientific	Cat#: 31985047
Lipofectamine RNAiMAX Transfection Reagent	ThermoFisher Scientific	Cat#: 13778075
Critical Commercial Assays		
SensiFAST cDNA Synthesis Kit	Bioline	Cat#: BIO-65054
SensiFAST Sybr Hi-ROX kit	Bioline	Cat#: BIO-92005
DC protein Assay Kit II	Bio-rad	Cat#: 5000111
CellTrace CFSE Cell Proliferation Kit	ThermoFisher Scientific	Cat#: C34570
Trans-Blot Turbo Mini Nitrocellulose Transfer Packs	Bio-rad	Cat#: 1704158

Maxima Probe/ROX qPCR Master Mix (2x)	ThermoFischer Scientific	Cat#: K0231
Kit for Creatinine detection	Spinreact	Cat#: 1001113
Kit for GOT/AST detection	Spinreact	Cat#: 1001162
Kit for GPT/ALT detection	Spinreact	Cat#: 41282
Kit for Cholesterol detection	Spinreact	Cat#: 1001093
Kit for HDL detection	Spinreact	Cat#: 1001098
Kit for LDL detection	Spinreact	Cat#: 41023
Kit for Urea detection	Spinreact	Cat#: 41043
Kit for Triglycerides detection	Spinreact	Cat#: 1001314
Kit for Acetic Acid detection (ACS Analyser Format)	Megazyme	Cat#: K-ACETAF
KASP V4.0 2X Mastermix 96/384, Low Rox	LGC Group	Cat#: KBS-1016-002
KASP by Design (KBD) Primer Mix (for <i>HIF1A</i> rs2057482 and <i>HIF1A</i> rs11519465)	LGC Group	https://www.lgcgroup.com/products/kasp-genotyping-chemistry/reagents/kbd/#.W7SDMi9Qqfc
TNF alpha Mouse Uncoated ELISA Kit with Plates	Invitrogen	Cat#: 88-7324-22
IL-6 Mouse Uncoated ELISA Kit with Plates	Invitrogen	Cat#: 88-7064-22
IL-10 Mouse Uncoated ELISA Kit with Plates	Invitrogen	Cat#: 88-7105-22
Silencer Select <i>Bnip3</i> siRNA	ThermoFisher Scientific	Cat#: 4390771
Experimental Models: Organisms/Strains		
C57BL/6J mice	Jackson Laboratories	Cat#: 000664
C57BL/6-Ly5.1 mice	Dr. Cláudia Nóbrega and Dr. Margarida Correia-Neves (ICVS, Braga)	N/A
BALB/c mice	Dr. Bhaskar Saha (NCCS, Pune)	N/A
129/Sv mice	Dr. Bhaskar Saha (NCCS, Pune)	N/A
mHIF-1 α ^{-/-} mice	Prof. Rui Appelberg (IBMC, Porto)	N/A
<i>Leishmania donovani</i> MHOM/IN/82/Patra 1	Dr. Baptiste Vergnes (IRD, Montpellier)	N/A
<i>Leishmania infantum</i> ITMAP 263	Dr. Baptiste Vergnes (IRD, Montpellier)	N/A
<i>Leishmania donovani</i> MHOM/ IN/83/AG83	Dr. Bhaskar Saha (NCCS, Pune)	N/A
Oligonucleotides (refer to table S1)		
Software and Algorithms		
GraphPad Prism v6	GraphPad Software	https://www.graphpad.com
FlowJo	FlowJo LLC	https://www.flowjo.com
CFX Manager	Bio-rad	http://www.bio-rad.com/en-pt/product/cfx-manager-software?ID=aed9803d-cb4d-4ecb-9263-3efc9e650edb
Fiji	ImageJ	https://fiji.sc
Other		
CD14 Microbeads, human	MACS Miltenyi Biotec	Cat#: 130-097-052

MS columns	MACS Miltenyi Biotec	Cat#: 130-041-301
BODIPY 493/503	ThermoFisher Scientific	Cat#: D3922
BODIPY FL C16	ThermoFisher Scientific	Cat#: D3821
DAF-FM Diacetate	ThermoFisher Scientific	Cat#: D23844
DAPI (4',6-Diamidino-2-Phenylindole, Dihydrochloride)	ThermoFisher Scientific	Cat#: D1306
Lab Vision™ PermaFluor™ Aqueous Mounting Medium	ThermoFisher Scientific	Cat#: TA-030-FM
HPTLC silica gel 60 (25 aluminium sheets)	Merck	Cat#: 1.05547.0001
MicroAmp Fast Optical 96-well reaction plate	Applied Biosystems by Life Technologies	Cat#: 4346906
Multiplate PCR Plates 96-well, clear	Bio-rad	Cat#: MLL9601

Lead Contact and Materials Availability

Further information and requests for resources and reagents should be directed to and will be fulfilled by the Lead Contact, Ricardo Silvestre (ricardosilvestre@med.uminho.pt) This study did not generate new unique reagents. There are no restrictions to the availability of data generated in this study.

Experimental model and subject details

Mice

Wild-type (WT) C57BL/6 were purchased from Charles River Laboratories and *Hif1α^{flox/flox}* mice crossed with lysozyme M-driven Cre (*LysM^{Cre}*)-transgenic mice on a C57BL/6 background, here identified as myeloid-restricted HIF-1α deficient mice (mHIF-1α^{-/-}), were kindly provided by Dr. Rui Appelberg (I3S; Porto, Portugal). C57BL/6 WT, mHIF-1α^{-/-} mice, BALB/c and 129/SV were bred and maintained in accredited animal facilities at the Life and Health Sciences Research Institute (ICVS). Mice were housed in groups of 3-6, in HEPA filter-bearing cages, under 12-h light/dark cycles. Autoclaved chow and water were provided *ad libitum* and cages were enriched with nesting materials (paper towels). Males and females with 8-12 weeks were used. Due to colony management and animal availability, all the *in vitro* experiments were performed with males while *in vivo* infection experiments were performed with mixed-gender groups (Table S2-3). Experimental animal procedures agreed with the European Council Directive (2010/63/EU) guidelines that were transposed into Portuguese law (Decree-Law n.º113/2013, August 7th). Experiments were conducted with the approval

of the UMinho Ethical Committee (process no. SECVS 074/2016) and complied with the guidelines of the Committee and National Council of Ethics for the Life Sciences (CNECV). RS has an accreditation for animal research given from Portuguese Veterinary Direction (Ministerial Directive 1005/92).

Parasite culture and staining

Cloned lines of virulent *Leishmania donovani* (MHOM/IN/82/Patra1 and MHOM/IN/83/AG83) and *L. infantum* (ITMAP 263) were maintained with weekly subpassages at 27°C in complete RPMI 1640 medium, supplemented with 10% heat-inactivated fetal bovine serum, 2 mM L-glutamine, 100 U/ml penicillin plus 100 mg/ml streptomycin and 20 mM HEPES buffer. Only parasites under ten passages were used in the experimental work. *L. donovani* promastigotes were stained with carboxyfluorescein succinimidyl ester (CFSE). Briefly, parasites were centrifuged and washed with warm phosphate-buffered saline (PBS) twice and then labelled with 5 µM CFSE (10×10^6 parasites/ml of PBS) for 10 minutes, at 37°C. The parasites were subsequently washed twice with PBS to quench the excess of fluorescence and suspended in complete RPMI.

Macrophage culture and *in vitro* infections

For peritoneal macrophages, peritoneal exudate was recovered after injection of ice-cold PBS in the peritoneal cavity. Cells were washed, resuspended in complete RPMI and plated at a density of 1×10^6 /ml. Non-adherent cells were removed through washing 4 hours after plating.

Bone marrow precursors from WT and HIF-1 $\alpha^{-/-}$ mice were recovered and differentiated in macrophages using recombinant M-CSF. Precursors were plated at 0.5×10^6 cells/ml with 20 ng/ml of M-CSF. Growth factor was renewed at day 4 post-differentiation. The macrophages were used 7 days after differentiation.

Peripheral blood mononuclear cells (PBMCs) were enriched from blood from healthy volunteers using a density gradient with Histopaque 1077. The mononuclear phase was recovered and washed with PBS. Next, cells were labelled with magnetic CD14 MicroBeads and CD14⁺ monocytes were positively separated using an MS column. Human CD14⁺ monocytes were differentiated in macrophages using recombinant M-CSF. Briefly, monocytes were plated at 1×10^6 cells/ml with 20 ng/ml of M-CSF.

Growth factor was renewed at day 4 post-differentiation. The macrophages were used 7 days after differentiation.

Macrophages were infected with *L. donovani* promastigotes at a 1:10 ratio. After 4 hours of incubation, non-phagocytosed parasites were removed, and cells were recovered. Macrophages were treated with C75 (40 μ M), sorA (500 nM) or deferoxamine (DFX; 500 μ M), 24 hours post-infection, for two hours, or left untreated as control. Following drug treatment, macrophages were left in culture for 4 days. Fatostatin A (10 μ M) was added 24 hours post-infection and left until analysis at day 5 post-infection. To assess if these drugs have a direct effect on the parasites, axenic promastigotes (starting with 1×10^6 parasites/ml) were treated with C75, fatostatin A and sorA and cultured until stationary phase. Parasites were fixated with 2% PFA and counted daily, for 4 days, using a Neubauer chamber. No major alterations were found, suggesting that the used drugs do not impact on parasite biology (figure S7C).

Method details

Parasite viability

Five days post-infection, the parasite viability was performed by adapting the Parasite Rescue Transformation Assay (Jain *et al.*, 2012). Briefly, culture media was renewed, and the plates were further sealed and placed in an incubator at 27°C to allow the conversion of amastigotes in promastigotes. The parasites were counted as abovementioned upon 7 days of incubation at 27°C. Similar results were obtained in parallel by following the rescue protocol (Jain *et al.*, 2012) and giemsa staining counting.

SNP selection and genotyping

The rs2057482 single nucleotide polymorphism (SNP) analyzed was selected based on their putative functional consequences. Genomic DNA was isolated from whole blood using the QIAcube automated system. Genotyping was performed using KASPar assays in an Applied Biosystems 7500 Fast Real-Time PCR system. Quality control for the genotyping results was achieved with negative controls and randomly selected samples with known genotypes.

Experimental *Leishmania* infection

Mice were infected with 10×10^6 (intravenous route) or 100×10^6 (intraperitoneal route) stationary *L. donovani* promastigotes. Weight and general well-being were monitored during the infection. FASN inhibitor C75 was administered via intraperitoneal route, at days 2, 4, 6 and 8 post-infection (10 mg/kg). Control animals were equally injected with vehicle (sterile PBS with 5% DMSO). Fatostatin A was administered via intraperitoneal route at days 3, 4, 5 and 6 post-infection (15 mg/kg). Control animals were equally injected with vehicle (sterile corn oil with 5% DMSO). Mice were anesthetized with volatile isoflurane and blood was withdrawn by cardiac puncture. Euthanasia by cervical dislocation was performed following this procedure. The bone marrow, liver and spleen were recovered for further analysis. The bone marrow was flushed from the femurs and tibias and precursors were washed with PBS and frozen for DNA extraction. The liver and spleen were mechanically resuspended and cells were recovered for flow cytometry and DNA extraction. Liver cell suspensions were subjected to a Percoll gradient (40/80) to isolate hepatic leukocytes. DNA was extracted using the phenol-chloroform-isoamyl alcohol method. Briefly, an aqueous suspension with approximately 1×10^6 cells was mixed with a mixture of phenol-chloroform-isoamyl alcohol (25:24:1). After centrifugation, the aqueous phase was recovered and incubated overnight with 3M sodium acetate and absolute ethanol. The DNA pellet was washed twice with 70% ethanol and resuspended in RNase/DNase-free water. Parasite burden was assessed, using a TaqMan-based qPCR assay for detection and quantification of *L. donovani* kinetoplastid DNA. Total cholesterol, triglycerides, LDL, HDL, acetate, creatine, urea, ALT and AST levels were quantified in the serum using an AutoAnalyzer, using reagents from the same provider.

Oil Red O staining

The liver was perfused with saline solution (portal vein perfusion) and fixed overnight with 10% (w/v) formalin. The samples were then embedded in Tissue-Tek O.C.T. compound and frozen in liquid nitrogen. After sample section on the cryostat (8 μm), the slides were stained with Oil Red O solution and bright field images were acquired on a BX6 microscope.

Flow cytometry

Bodipy 493/503 (3 µg/ml) and Bodipy FL C16 (1 µM) were diluted in complete media and added to adherent cells for 30 minutes at 37°C. DAF-FM (2 µg/ml) was diluted in PBS and incubated for 30 minutes at 37°C. The cells were then washed with PBS, detached and analysed. Before analysis, cells stained with DAF-FM were left to rest for 20 minutes, to complete de-esterification of intracellular diacetates. Surface staining was performed with the following antibodies: BV605 anti-mouse CD11c, clone N418; APC anti-mouse I-A/I-E, clone M5/114.15.2; BV785 anti-mouse NK1.1, clone PK136; PE/Cy7 anti-mouse CD11b, clone M1/70; BV711 anti-mouse Ly6G, clone 1A8; PerCP/Cy5.5 anti-mouse Ly6C, clone HK14. Samples were acquired on a LSRII flow cytometer (BD Biosciences) and data analysed using FlowJo software. The gating strategy for myeloid cells is depicted on Supplementary Figure 7D.

High performance liquid chromatography

Glucose and lactate were quantified in cell culture supernatant using HPLC technology (Gilson bomb system); HyperREZ XP Carbohydrate H+ 8µM. Samples were filtered with a 0.2 µm filter and the mobile phase (0.0025M H₂SO₄) was similarly filtered and degasified for 30 minutes. Each sample was analyzed using the following running protocols (sensitivity 8): 15 minutes at a constant flux of 0.7 ml/min at 54°C for glucose and lactate detection. The peaks were detected in a refractive index detector (IOTA 2, Reagents) and integration was performed using Gilson Uniprot Software, version 5.11.

Lipid extraction and HPTLC analysis

Lipid extraction was performed using a modified Bligh and Dyer (1959) methodology. Macrophages were lysed in ice-cold lysis buffer containing 50 mM Tris, pH 7.4, 1% Triton X-100, 150 mM NaCl, 10% glycerol, 50 mM NaF, 5 mM sodium pyrophosphate, 1 mM Na₃VO₄, 25 mM sodium-β-glycerophosphate, 1 mM DTT, 0.5 mM PMSF and protease inhibitors. A chloroform-methanol-water solution (2:1:0.8 v/v) was added to the lysates (70µg), which were left in intermittent shaking for two hours. The initial phases were separated by centrifugation (730g, 20 min at 4°C) and the supernatant was collected. A water-chloroform solution (1:1) was added to the supernatant and the organic phase was collected after centrifugation (730g, 20 min at 4°C). The extracted lipids were analyzed by high performance thin layer chromatography (HPTLC) using

hexane-diethyl ether-acetic acid solvent (60:40:1 v/v). For detection, the plates were sprayed in a carbonization solution with 8% CuSO₄ and 10% H₃PO₄ and heated at 110°C for 20 minutes. The lipid bands were then analyzed by densitometry using the Fiji software.

Quantitative PCR analysis

Total RNA was isolated from cells with TRI reagent, according to the manufacturer instructions. RNA concentration was determined by OD260 measurement using a NanoDrop spectrophotometer. Total RNA (10-200ng) was reverse-transcribed using the SensiFAST cDNA Synthesis Kit. Real-Time quantitative PCR (qRT-PCR) reactions were run for each sample on a Bio-Rad CFX96 Real-Time System C1000 Thermal Cycler. Primer sequences were obtained from Alfagene and thoroughly tested. The RT product was expanded using the SensiFAST SYBR Hi-ROX kit and the results were normalized to the expression of the housekeeping gene *18s*. After amplification, cycle threshold-values (Ct-values) were calculated for all samples and gene expression changes were analyzed in the CFX Manager Software.

Western blot

Approximately $1-4 \times 10^6$ macrophages were lysed in ice-cold lysis buffer containing 50 mM Tris, 0.25 M NaCl, 2 mM EDTA, 1% NP-40, 10% glycerol, complemented with protease/phosphatase cocktail inhibitor. The samples were left resting on ice for 30 minutes and then sonicated in an ultrasonic bath for additional 30 minutes. Following centrifugation (13.000g, 30 minutes, at 4°C), the lysates (ten to twenty-five micrograms of protein) were subjected to SDS-PAGE electrophoresis and the proteins were transferred to mini nitrocellulose membranes by the Trans Blot Turbo Transfer System. The membranes were then incubated with primary antibodies (1/1000 for each primary antibody) and with horseradish peroxidase-coupled secondary reagents. Detection was made with SuperSignal West Femto Maximum Sensitivity Substrate. Primary antibodies were directed against BNIP3, Phospho-p70 S6k kinase (Thr389), p70 S6 kinase, FASN and β -actin.

Enzyme-linked Immunosorbent Assay

The levels of cytokines were determined in the supernatant of WT and HIF-1 α ^{-/-} macrophages, 5 days post-infection, using TNF- α , IL-6 and IL-10 Mouse ELISA, following manufacturer's instructions.

Macrophage transfection

Bone marrow-derived macrophages were differentiated, as previously described. At the 7th day of differentiation, BNIP3 silencing was induced, using small interfering RNA (siRNA) technology. Briefly, a lipid-based transfection was performed with Lipofectamine RNAiMAX Transfection Reagent. The siRNA/lipid complexes were added to macrophage culture during 4h, in Opti-MEM Reduced Serum Media. Then, the complexes were removed and cells were left resting in complete RPMI for 14 hours. Cell viability was unaltered in BNIP3-silenced conditions, when compared to scramble control and untransfected cells. Macrophage infection was performed as already described and samples were stored for western blot and quantitative PCR, 10 and 24 hours post-infection, respectively.

Immunofluorescence

Peritoneal macrophages were cultured and infected in coverslips, as abovementioned. Upon 24 hours of infection, cells were fixated during 30 minutes with 10% formalin, at room temperature. Next, ice-cold methanol was added for ten minutes and cells were washed three times with PBS. To block non-specific antibody binding, the coverslips were incubated for one hour with 10% bovine serum albumin, at room temperature. The primary rabbit anti-SREBP-1c antibody was incubated at room temperature for two hours (1/200). The coverslips were washed three times with PBS. The secondary Alexa Fluor 488-labelled goat anti-rabbit IgG (H+L) antibody was incubated during one hour at room temperature. Following three washes with PBS, the nuclei were stained with DAPI during 10 minutes. The coverslips were mounted in Permafluor Mountant and appropriately sealed. Images were acquired on an Olympus FluoView FV1000 confocal laser scanning microscope.

Nuclear Magnetic Resonance

Bone marrow-derived macrophages from WT and mHIF-1 α ^{-/-} mice were cultured in the presence of 5 mM sodium acetate-2-¹³C for 24 hours, 3 days post-infection. The

cells were recovered and washed twice with PBS. After centrifugation, the pellet was resuspended in methanol (4 ml/g of cells) and water (0.85 ml/g of cells) and left on ice for 10 minutes. Chloroform (4 ml/g of cells) and water (2 ml/g of cells) were then added, followed by an additional 10 minutes on ice. The organic and aqueous phases were separated by centrifugation and stored at -80°C. After solvent evaporation in a speed-vacuum concentrator, the aqueous phases were suspended in 600 μ L D₂O containing 2 mM NaN₃ and 0.29 mM TSP. All NMR experiments were performed at 25°C in a Bruker Avance II+ spectrometer, operating at a frequency of 800.33 MHz for ¹H, equipped with a 5 mm three channel probe (TXI-Z H/C/N/-D). For all samples were acquired: an ¹H-NMR spectra (*noesygppr1d* pulse program, with 64 k points, 96 scans, using a spectral window of 20.55 ppm, 4 s relaxation delay and 10 ms mixing time) and a ¹H-¹³C Heteronuclear Single Quantum Coherence spectra (*hsqcetgpsisp2* pulse program, with 512 points in F1 and 2048 points in F2, 128 scans, using a sweep width of 165 ppm in F1 and 16 ppm in F2 and 1.5 s relaxation delay). Spectra processing was performed using Topspin3.2 software and the resonances volumes on the ¹H-¹³C-HSQC spectra were determined using the same software.

Cell sorting

Peritoneal macrophages from Ly5.1 WT and mHIF-1 α ^{-/-} mice were co-cultured for two hours (1:1 ratio) and infected with *L. donovani*, as previously described. At the fifth day of infection, macrophages were recovered by detachment with a solution of 10 mM ethylenediaminetetraacetic acid (EDTA). Surface staining with PE anti-mouse CD45.1, clone A20 and APC anti-mouse CD45.2, clone 104 was performed and cells were sorted using BD FACSAria II. A similar number of purified WT and HIF-1 α ^{-/-} macrophages were used to assess parasite viability.

RNA sequencing

Reads were trimmed using Trimmomatic v0.36 with the following options: TRAILING:30, SLIDINGWINDOW:4:20 and MINLEN:30. All other options used the default values. Quality check was performed on raw and trimmed data to ensure the quality of the reads using FastQC v0.11.5 and MultiQC v1.5. The quantification was performed with Kallisto v0.44. Differential expression analysis was performed in R v3.5.0 using the DESeq2 v1.20.0 and volcano plots were produced with the ggplot2 package.

Quantification and statistical analysis

Statistical analyses were performed with the GraphPad Prism 6 software. A one-way analysis of variance (ANOVA) followed by a Bonferroni's post hoc test was employed for multiple group comparisons. A Mann-Whitney test of variance and Kruskal-Wallis non-parametric test were performed accordingly with the correspondent experimental design. The statistical details of each experiment can be found in figure legends and the data is presented as mean \pm SD. Statistically significant values are as follows: * $p < 0.05$, ** $p < 0.01$, *** $p < 0.001$.

Data and Code Availability

The RNAseq data generated during this study are available at Gene Expression Omnibus (GEO) under the accession number GSE145136.

References

- Abram, C. L. *et al.* (2014) 'Comparative analysis of the efficiency and specificity of myeloid-Cre deleting strains using ROSA-EYFP reporter mice', *Journal of Immunological Methods*, 408, pp. 89–100. doi: 10.1016/j.jim.2014.05.009.
- Alonso, D. *et al.* (2019) 'HIF-1 α -regulated MIF activation and Nox2-dependent ROS generation promote *Leishmania amazonensis* killing by macrophages under hypoxia', *Cellular Immunology*. doi: 10.1016/j.cellimm.2018.10.007.
- Bailey, A. P. *et al.* (2015) 'Antioxidant Role for Lipid Droplets in a Stem Cell Niche of *Drosophila*', *Cell*, 163, pp. 340–353. doi: 10.1016/j.cell.2015.09.020.
- Becker, I. *et al.* (2003) 'Leishmania lipophosphoglycan (LPG) activates NK cells through toll-like receptor-2', *Molecular and Biochemical Parasitology*, 130(2), pp. 65–74. doi: 10.1016/S0166-6851(03)00160-9.
- Bensaad, K. *et al.* (2014) 'Fatty acid uptake and lipid storage induced by HIF-1 α contribute to cell growth and survival after hypoxia-reoxygenation', *Cell Reports*, 9(1), pp. 349–365. doi: 10.1016/j.celrep.2014.08.056.
- Berod, L. *et al.* (2014) 'De novo fatty acid synthesis controls the fate between regulatory T and T helper 17 cells', *Nature Medicine*, 20(11). doi: 10.1038/nm.3704.
- Blume, M. *et al.* (2015) 'A *Toxoplasma gondii* gluconeogenic enzyme contributes to robust central carbon metabolism and is essential for replication and virulence', *Cell Host and Microbe*, 18(2), pp. 210–220. doi: 10.1016/j.chom.2015.07.008.
- Bodhale, N. P. *et al.* (2018) 'Inbred mouse strains differentially susceptible to *Leishmania donovani* infection differ in their immune cell metabolism', *Cytokine*. doi: 10.1016/j.cyto.2018.06.003.
- Bozza, P. T. *et al.* (2009) 'Lipid droplets in host-pathogen interactions', *Clinical Lipidology*, 4(6), pp. 791–807. doi: 10.2217/clp.09.63.
- Caradonna, K. L. *et al.* (2013) 'Host metabolism regulates intracellular growth of *Trypanosoma cruzi*', *Cell Host and Microbe*, 13(1), pp. 108–117. doi: 10.1016/j.chom.2012.11.011.
- Caron, A., Richard, D. and Laplante, M. (2015) 'The Roles of mTOR Complexes in Lipid Metabolism', *Annual Review of Nutrition*. doi: 10.1146/annurev-nutr-071714-034355.
- Chang, Y. *et al.* (2006) 'Keratinocyte growth factor induces lipogenesis in alveolar type II cells through a sterol regulatory element binding protein-1c-dependent pathway', *American Journal of Respiratory Cell and Molecular Biology*. doi:

10.1165/rcmb.2006-0037OC.

Cheng, S.-C. *et al.* (2014) 'mTOR- and HIF-1 -mediated aerobic glycolysis as metabolic basis for trained immunity', *Science*, 345(6204), pp. 1250684–1250684. doi: 10.1126/science.1250684.

Chinnadurai, G., Vijayalingam, S. and Gibson, S. B. (2008) 'BNIP3 subfamily BH3-only proteins: Mitochondrial stress sensors in normal and pathological functions', *Oncogene*. doi: 10.1038/onc.2009.49.

Choudhry, H. and Harris, A. L. (2017) 'Advances in Hypoxia-Inducible Factor Biology', *Cell Metabolism*. doi: 10.1016/j.cmet.2017.10.005.

De Cicco, N. N. T. *et al.* (2012) 'LDL uptake by *Leishmania amazonensis*: Involvement of membrane lipid microdomains', *Experimental Parasitology*, 130(4), pp. 330–340. doi: 10.1016/j.exppara.2012.02.014.

Cramer, T. *et al.* (2003) 'HIF-1 α is essential for myeloid cell-mediated inflammation', *Cell*, 112(5), pp. 645–657. doi: 10.1016/S0092-8674(03)00154-5.

Degrossoli, A. *et al.* (2007) 'Expression of hypoxia-inducible factor 1 α in mononuclear phagocytes infected with *Leishmania amazonensis*', *Immunology Letters*, 114(2), pp. 119–125. doi: S0165-2478(07)00240-4 [pii]n10.1016/j.imlet.2007.09.009.

Du, W. *et al.* (2017) 'HIF drives lipid deposition and cancer in ccRCC via repression of fatty acid metabolism', *Nature Communications*, 8(1). doi: 10.1038/s41467-017-01965-8.

Düvel, K. *et al.* (2010) 'Activation of a metabolic gene regulatory network downstream of mTOR complex 1', *Molecular Cell*. doi: 10.1016/j.molcel.2010.06.022.

Eberlé, D. *et al.* (2004) 'SREBP transcription factors: Master regulators of lipid homeostasis', *Biochimie*, pp. 839–848. doi: 10.1016/j.biochi.2004.09.018.

Feingold, K. R. *et al.* (2012) 'Mechanisms of triglyceride accumulation in activated macrophages', *Journal of Leukocyte Biology*, 92(4), pp. 829–839. doi: 10.1189/jlb.1111537.

Flavin, R. *et al.* (2010) 'Fatty acid synthase as a potential therapeutic target in cancer.', *Future oncology (London, England)*, 6(4), pp. 551–62. doi: 10.2217/fon.10.11.

Ghosh, A. K. *et al.* (2015) 'Metabolic reconfiguration of the central glucose metabolism: A crucial strategy of *Leishmania donovani* for its survival during

oxidative stress', *FASEB Journal*, 29(5), pp. 2081–2098. doi: 10.1096/fj.14-258624.

Guo, X. *et al.* (2015) 'SNP rs2057482 in HIF1A gene predicts clinical outcome of aggressive hepatocellular carcinoma patients after surgery', *Scientific Reports*, 5. doi: 10.1038/srep11846.

Hammami, A. *et al.* (2017) 'HIF-1 α is a key regulator in potentiating suppressor activity and limiting the microbicidal capacity of MDSC-like cells during visceral leishmaniasis', *PLoS Pathogens*. doi: 10.1371/journal.ppat.1006616.

Hlatky, M. A. *et al.* (2007) 'Polymorphisms in hypoxia inducible factor 1 and the initial clinical presentation of coronary disease', *American Heart Journal*, 154(6), pp. 1035–1042. doi: 10.1016/j.ahj.2007.07.042.

Horton, J. D., Goldstein, J. L. and Brown, M. S. (2002) 'SREBPs: Activators of the complete program of cholesterol and fatty acid synthesis in the liver', *Journal of Clinical Investigation*, pp. 1125–1131. doi: 10.1172/JCI0215593.

Howard, B. V (1977) 'Acetate as a carbon source for lipid synthesis in cultured cells.', *Biochimica et biophysica acta*, 488(1), pp. 145–51. doi: 10.1016/0005-2760(77)90132-1.

Idrovo, J. P. *et al.* (2015) 'Inhibition of lipogenesis reduces inflammation and organ injury in sepsis', *Journal of Surgical Research*, 200(1), pp. 242–249. doi: 10.1016/j.jss.2015.06.059.

Imtiyaz, H. Z. and Simon, M. C. (2010) 'Hypoxia-inducible factors as essential regulators of inflammation', *Current Topics in Microbiology and Immunology*, 345(1), pp. 105–120. doi: 10.1007/82-2010-74.

Jain, S. K. *et al.* (2012) 'A parasite rescue and transformation assay for antileishmanial screening against intracellular *Leishmania donovani* amastigotes in THP1 human acute monocytic leukemia cell line.', *Journal of visualized experiments : JoVE*. doi: 10.3791/4054.

Joseph, S. B. *et al.* (2002) 'Direct and indirect mechanisms for regulation of fatty acid synthase gene expression by liver X receptors', *Journal of Biological Chemistry*, 277(13), pp. 11019–11025. doi: 10.1074/jbc.M111041200.

Kim, H. O. *et al.* (2008) 'The C1772T genetic polymorphism in human HIF-1 α gene associates with expression of HIF-1 α protein in breast cancer', *Oncol Rep*, 20(5), pp. 1181–1187. doi: 10.3892/or.

Kropf, P. *et al.* (2004) 'Toll-Like Receptor 4 Contributes to Efficient Control of Infection with the Protozoan Parasite *Leishmania major*', *Infection and Immunity*,

72(4), pp. 1920–1928. doi: 10.1128/IAI.72.4.1920-1928.2004.

Kuhajda, F. P. *et al.* (2000) ‘Synthesis and antitumor activity of an inhibitor of fatty acid synthase.’, *Proceedings of the National Academy of Sciences of the United States of America*, 97(7), pp. 3450–4. doi: 10.1073/pnas.050582897.

Kuncewitch, M. *et al.* (2016) ‘Inhibition of fatty acid synthase with C75 decreases organ injury after hemorrhagic shock’, *Surgery*, 159(2), pp. 570–579. doi: 10.1016/j.surg.2015.07.036.

Laplante, M. and Sabatini, D. M. (2009) ‘An Emerging Role of mTOR in Lipid Biosynthesis’, *Current Biology*. doi: 10.1016/j.cub.2009.09.058.

Lee, J.-W. *et al.* (2004) ‘Hypoxia-inducible factor (HIF-1)alpha: its protein stability and biological functions.’, *Experimental & molecular medicine*, 36(1), pp. 1–12. doi: 10.1038/emm.2004.1.

Li, Y. *et al.* (2007) ‘Bnip3 mediates the hypoxia-induced inhibition on mammalian target of rapamycin by interacting with Rheb’, *Journal of Biological Chemistry*, 282(49), pp. 35803–35813. doi: 10.1074/jbc.M705231200.

Liu, L. *et al.* (2015) ‘Glial lipid droplets and ROS induced by mitochondrial defects promote neurodegeneration’, *Cell*, 160(1–2), pp. 177–190. doi: 10.1016/j.cell.2014.12.019.

Liu, N., Qiao, K. and Stephanopoulos, G. (2016) ‘¹³C Metabolic Flux Analysis of acetate conversion to lipids by *Yarrowia lipolytica*’, *Metabolic Engineering*, 38, pp. 86–97. doi: 10.1016/j.ymben.2016.06.006.

Liu, Y. *et al.* (2014) ‘HIF-1 α and HIF-2 α are critically involved in hypoxia-induced lipid accumulation in hepatocytes through reducing PGC-1 α -mediated fatty acid β -oxidation’, *Toxicology Letters*, 226(2), pp. 117–123. doi: 10.1016/j.toxlet.2014.01.033.

Lu, H., Forbes, R. A. and Verma, A. (2002) ‘Hypoxia-inducible factor 1 activation by aerobic glycolysis implicates the Warburg effect in carcinogenesis.’, *The Journal of biological chemistry*, 277(26), pp. 23111–5. doi: 10.1074/jbc.M202487200.

Mao, Z. and Zhang, W. (2018) ‘Role of mTOR in Glucose and Lipid Metabolism’, *International Journal of Molecular Sciences*. doi: 10.3390/ijms19072043.

Marin-Hernandez, A. *et al.* (2009) ‘HIF-1 α ; Modulates Energy Metabolism in Cancer Cells by Inducing Over-Expression of Specific Glycolytic Isoforms’, *Mini-Reviews in Medicinal Chemistry*, 9(9), pp. 1084–1101. doi: 10.2174/138955709788922610.

- Matsuo, S. *et al.* (2014) 'Fatty acid synthase inhibitor C75 ameliorates experimental colitis.', *Molecular medicine (Cambridge, Mass.)*, 20, pp. 1–9. doi: 10.2119/molmed.2013.00113.
- McConville, M. J. (2016) 'Metabolic Crosstalk between Leishmania and the Macrophage Host', *Trends in Parasitology*, pp. 666–668. doi: 10.1016/j.pt.2016.05.005.
- McGettrick, A. F. *et al.* (2016) 'Trypanosoma brucei metabolite indolepyruvate decreases HIF-1 α and glycolysis in macrophages as a mechanism of innate immune evasion', *Proceedings of the National Academy of Sciences*, 113(48), pp. E7778–E7787. doi: 10.1073/pnas.1608221113.
- Moreira, D. *et al.* (2015) 'Leishmania infantum Modulates Host Macrophage Mitochondrial Metabolism by Hijacking the SIRT1-AMPK Axis', *PLoS Pathogens*, 11(3), pp. 1–24. doi: 10.1371/journal.ppat.1004684.
- Murray, P. J. *et al.* (2014) 'Macrophage Activation and Polarization: Nomenclature and Experimental Guidelines', *Immunity*, pp. 14–20. doi: 10.1016/j.immuni.2014.06.008.
- Na, Y. R. *et al.* (2016) 'GM-CSF Induces Inflammatory Macrophages by Regulating Glycolysis and Lipid Metabolism', *The Journal of Immunology*, 197(10), pp. 4101–4109. doi: 10.4049/jimmunol.1600745.
- Naderer, T. and McConville, M. J. (2008) 'The Leishmania-macrophage interaction: A metabolic perspective', *Cellular Microbiology*, pp. 301–308. doi: 10.1111/j.1462-5822.2007.01096.x.
- Nath, B. *et al.* (2011) 'Hepatocyte-specific hypoxia-inducible factor-1 α is a determinant of lipid accumulation and liver injury in alcohol-induced steatosis in mice', *Hepatology*, 53(5), pp. 1526–1537. doi: 10.1002/hep.24256.
- Nicholas, S. A. and Sumbayev, V. V. (2009) 'The involvement of hypoxia-inducible factor 1 alpha in toll-like receptor 7/8-mediated inflammatory response', *Cell Research*, 19(8), pp. 973–983. doi: 10.1038/cr.2009.44.
- Nishiyama, Y. *et al.* (2012) 'HIF-1 α induction suppresses excessive lipid accumulation in alcoholic fatty liver in mice', *Journal of Hepatology*, 56(2), pp. 441–447. doi: 10.1016/j.jhep.2011.07.024.
- Nomura, M. *et al.* (2016) 'Fatty acid oxidation in macrophage polarization', *Nature Immunology*, pp. 216–217. doi: 10.1038/ni.3366.
- Palazon, A. *et al.* (2014) 'HIF Transcription Factors, Inflammation, and Immunity',

- Immunity*, pp. 518–528. doi: 10.1016/j.immuni.2014.09.008.
- Palsson-Mcdermott, E. M. *et al.* (2015) ‘Pyruvate kinase M2 regulates hif-1 α activity and il-1 β induction and is a critical determinant of the warburg effect in LPS-activated macrophages’, *Cell Metabolism*, 21(1), pp. 65–80. doi: 10.1016/j.cmet.2014.12.005.
- Peyssonaux, C. *et al.* (2007) ‘Cutting edge: Essential role of hypoxia inducible factor-1 alpha in development of lipopolysaccharide-induced sepsis’, *Journal of immunology*, 178(12), pp. 7516–7519. doi: 10.4049/JIMMUNOL.178.12.7516.
- Porstmann, T. *et al.* (2008) ‘SREBP Activity Is Regulated by mTORC1 and Contributes to Akt-Dependent Cell Growth’, *Cell Metabolism*. doi: 10.1016/j.cmet.2008.07.007.
- Rabhi, I. *et al.* (2012) ‘Transcriptomic Signature of Leishmania Infected Mice Macrophages: A Metabolic Point of View’, *PLoS Neglected Tropical Diseases*, 6(8). doi: 10.1371/journal.pntd.0001763.
- Rabhi, S. *et al.* (2016) ‘Lipid droplet formation, their localization and dynamics during leishmania major macrophage infection’, *PLoS ONE*, 11(2). doi: 10.1371/journal.pone.0148640.
- Raha, S. *et al.* (2016) ‘Disruption of de novo fatty acid synthesis via acetyl-CoA carboxylase 1 inhibition prevents acute graft-versus-host disease’, *European Journal of Immunology*, 46(9), pp. 2233–2238. doi: 10.1002/eji.201546152.
- Rahtu-Korpela, L. *et al.* (2014) ‘HIF prolyl 4-hydroxylase-2 inhibition improves glucose and lipid metabolism and protects against obesity and metabolic dysfunction’, *Diabetes*, 63(10), pp. 3324–3333. doi: 10.2337/db14-0472.
- Rahtu-Korpela, L. *et al.* (2016) ‘Hypoxia-Inducible Factor Prolyl 4-Hydroxylase-2 Inhibition Protects Against Development of Atherosclerosis’, *Arteriosclerosis, Thrombosis, and Vascular Biology*, 36(4), pp. 608–617. doi: 10.1161/ATVBAHA.115.307136.
- Rankin, E. B. *et al.* (2009) ‘Hypoxia-Inducible Factor 2 Regulates Hepatic Lipid Metabolism’, *MOLECULAR AND CELLULAR BIOLOGY*, 29(16), pp. 4527–4538. doi: 10.1128/MCB.00200-09.
- Rius, J. *et al.* (2008) ‘NF-kappaB links innate immunity to the hypoxic response through transcriptional regulation of HIF-1alpha.’, *Nature*, 453(7196), pp. 807–11. doi: 10.1038/nature06905.
- Riviere, L. *et al.* (2009) ‘Acetate produced in the mitochondrion is the essential precursor for lipid biosynthesis in procyclic trypanosomes’, *Proceedings of the*

- National Academy of Sciences*, 106(31), pp. 12694–12699. doi: 10.1073/pnas.0903355106.
- Rodrigues, V. *et al.* (2016) ‘Regulation of immunity during visceral Leishmania infection’, *Parasites and Vectors*. doi: 10.1186/s13071-016-1412-x.
- Rodríguez, N. E. *et al.* (2017) ‘Lipid bodies accumulation in Leishmania infantum-infected C57BL/6 macrophages’, *Parasite Immunology*, 39(8). doi: 10.1111/pim.12443.
- Schatz, V. *et al.* (2016) ‘Myeloid Cell–Derived HIF-1 α Promotes Control of *Leishmania major*’, *The Journal of Immunology*, 197(10), pp. 4034–4041. doi: 10.4049/jimmunol.1601080.
- Semini, G. *et al.* (2017) ‘Changes to cholesterol trafficking in macrophages by Leishmania parasites infection’, *MicrobiologyOpen*, 6(4). doi: 10.1002/mbo3.469.
- Silvestre, R. *et al.* (2009) ‘Recognition of Leishmania parasites by innate immunity’, *Immunology, Endocrine and Metabolic Agents in Medicinal Chemistry*, 9(2), pp. 106–127. doi: 10.2174/187152209789000713.
- Singh, A. K. *et al.* (2012) ‘Intracellular pathogen Leishmania donovani activates hypoxia inducible factor-1 by dual mechanism for survival advantage within macrophage’, *PLoS ONE*, 7(6). doi: 10.1371/journal.pone.0038489.
- Smith, T. K. *et al.* (2017) ‘Metabolic reprogramming during the Trypanosoma brucei life cycle’, *F1000Research*, 6, p. 683. doi: 10.12688/f1000research.10342.1.
- Sone, H. *et al.* (2015) ‘Acetyl-coenzyme A synthetase is a lipogenic enzyme controlled by SREBP-1 and energy status’, *American Journal of Physiology-Endocrinology and Metabolism*. doi: 10.1152/ajpendo.00189.2001.
- Spirig, R. *et al.* (2010) ‘Effects of TLR agonists on the hypoxia-regulated transcription factor HIF-1 α and dendritic cell maturation under normoxic conditions’, *PLoS ONE*, 5(6). doi: 10.1371/journal.pone.0010983.
- Thompson, C. B. (2016) ‘Into Thin Air: How We Sense and Respond to Hypoxia’, *Cell*, pp. 9–11. doi: 10.1016/j.cell.2016.08.036.
- Tuon, F. F. *et al.* (2008) ‘Toll-like receptors and leishmaniasis’, *Infection and Immunity*, pp. 866–872. doi: 10.1128/IAI.01090-07.
- Vats, D. *et al.* (2006) ‘Oxidative metabolism and PGC-1 β attenuate macrophage-mediated inflammation.’, *Cell metabolism*, 4(1), pp. 13–24. doi: 10.1016/j.cmet.2006.05.011.
- Wang, X. *et al.* (2016) ‘Single nucleotide polymorphism in the microRNA-199a

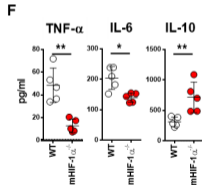
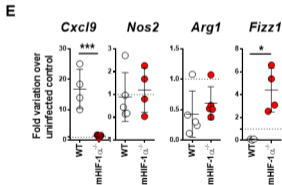
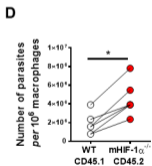
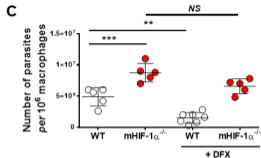
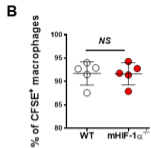
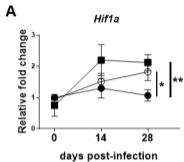
binding site of HIF1A gene is associated with pancreatic ductal adenocarcinoma risk and worse clinical outcomes', *Oncotarget*, 7(12). doi: 10.18632/oncotarget.7263.

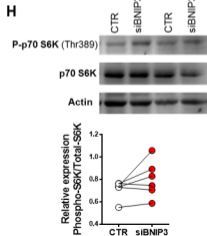
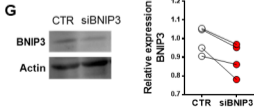
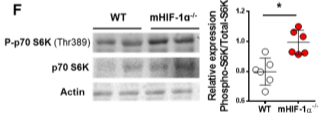
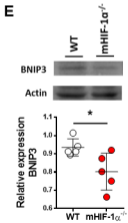
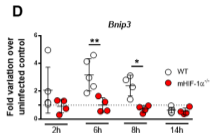
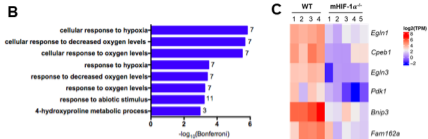
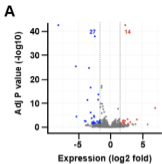
Weidemann, A. and Johnson, R. S. (2008) 'Biology of HIF-1 α ', *Cell Death and Differentiation*, pp. 621–627. doi: 10.1038/cdd.2008.12.

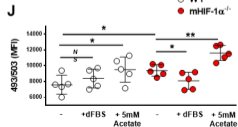
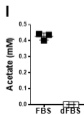
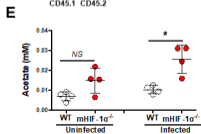
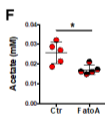
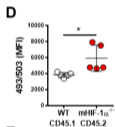
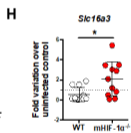
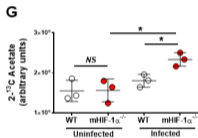
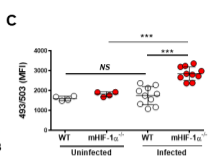
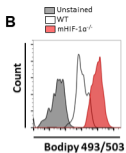
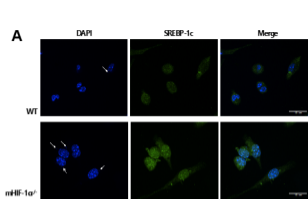
Werth, N. *et al.* (2010) 'Activation of hypoxia inducible factor 1 is a general phenomenon in infections with human pathogens', *PLoS ONE*, 5(7). doi: 10.1371/journal.pone.0011576.

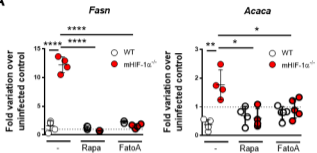
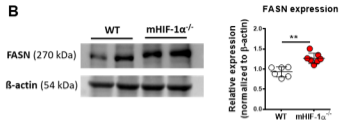
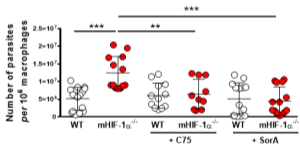
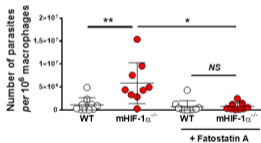
Xiao, X. and Song, B. (2013) 'SREBP: a novel therapeutic target', *Acta Biochimica et Biophysica Sinica*, 45(1), pp. 2–10. doi: 10.1093/abbs/gms112.

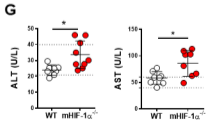
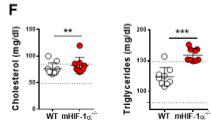
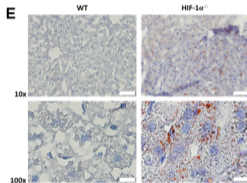
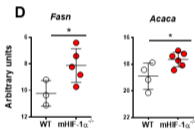
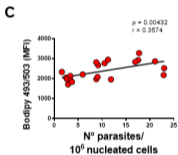
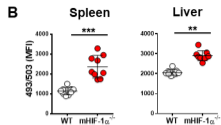
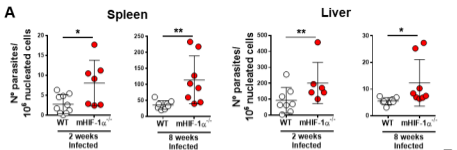
Zhang, X. *et al.* (2010) 'Adipose tissue-specific inhibition of hypoxia-inducible factor 1 α induces obesity and glucose intolerance by impeding energy expenditure in mice', *Journal of Biological Chemistry*, 285(43), pp. 32869–32877. doi: 10.1074/jbc.M110.135509.

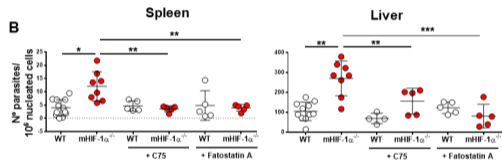
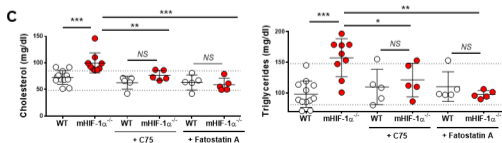


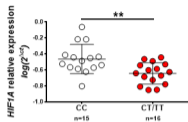
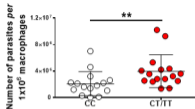
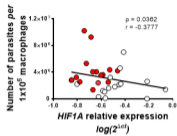
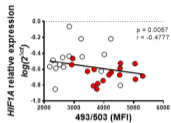
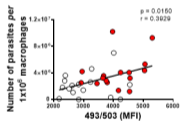
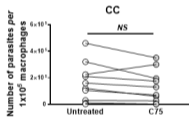
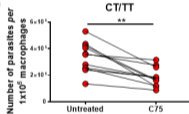





A**B****C****D**




A**B****C**

A**B****C****D****E****F****G**

Genetic
deficiency of HIF-1 α

 mHIF-1 α ^{-/-}
LysM Cre-specific
deletion of HIF-1 α

 SNP rs2057482
HIF-1 α
loss-of-function

